

Technical Report

Title: *Measurement of Diffusion Properties by X-Ray Radiography and by Through-Diffusion Techniques Using Iodide and Tritium Tracers: Core Samples from OS-1 and DGR-2*

Document ID: TR-07-17


Authors: Tom Al, Yan Xiang and Lisa Cavé
University of New Brunswick

Revision: 3

Date: May 19, 2010

DGR Site Characterization Document
Intera Engineering Project 06-219



Intera Engineering DGR Site Characterization Document	
Title:	Measurement of Diffusion Properties by X-Ray Radiography and by Through-Diffusion Techniques Using Iodide and Tritium Tracers: Core Samples from OS-1 and DGR-2.
Document ID:	TR-07-17
Revision Number:	3
	Date: May 19, 2010
Author(s):	Tom Al, Yan Xiang, Lisa Cavé (University of New Brunswick)
Technical Review:	Kenneth Raven; Monique Hobbs, Jennifer McKelvie, Laura Kennell (NWMO); Joe Pearson, Andreas Gautschi (GRG)
QA Review:	John Avis
Approved by:	 Kenneth Raven

Document Revision History		
Revision	Effective Date	Description of Changes
0	July 21, 2008	Initial issue
1	September 7, 2008	Revision of sample DGR2-746.33 as Kirkfield Formation, not Sherman Fall
2	February 3, 2009	The following revisions have been made: 1) A new equation [4] was added, and therefore the numbers of all subsequent equations increased by one. 2) Equation [5], previously equation 4, was modified. 3) The grain density data were re-calculated using new equation [5] and data in Table 5 were updated. 4) The identification codes (ID) of sub-samples in Table 5 were modified so that they are consistent with the ID used in electronic files. 5) The grain density data in Table 6 were updated and two typos were corrected. 6) Updated Table 2 formations (sample DGR2-614.47)

		to conform with results of November 2008 core workshop
3	May 19, 2010	Minor editorial changes to address NWMO comments

TABLE OF CONTENTS

1	INTRODUCTION	1
2	SAMPLE DESCRIPTIONS AND SUB-SAMPLING	1
3	METHODS	2
	3.1 Water-Loss Porosity	2
	3.2 Pore Water Composition	5
	3.3 Diffusion and Porosity Measurements – Radiography.....	5
	3.4 Diffusion Measurements – Through Diffusion	10
4	RESULTS AND DISCUSSION	12
	4.1 Water-Loss Porosity	12
	4.2 Pore Water Composition	13
	4.3 Diffusion and Porosity Measurements – Radiography.....	15
	4.4 Diffusion Measurements – Through Diffusion	18
	4.5 Comparison of Radiography and Through Diffusion.....	22
	4.6 Reproducibility of the TD Measurements	22
5	SUMMARY	23
6	DATA QUALITY AND USE	24
7	REFERENCES	24

LIST OF TABLES

Table 1	Description of OS-1 Limestone Core Samples Received from Intera	1
Table 2	Description of DGR-2 Rock Core Samples Received from Intera.....	3
Table 3	Sub Samples Cut From DGR-2 Rock Cores	4
Table 4	X-Ray Radiography Data Acquisition Parameters for OS-1 and DGR-2 Samples	6
Table 5	Water Loss Porosity and Grain Density	12
Table 6	Pore Water Composition Data.....	13
Table 7	SPW and Iodide-Tracer Solution Compositions for Diffusion Experiments.	15
Table 8	Diffusion-Coefficient and ϕ_i Data from X-Ray Radiography (22±1°C).....	16
Table 9	Diffusion Coefficient Data and Tracer-Accessible Porosity for DGR-2 Samples Determined Normal to Bedding by TD using 1.0 M NaI (23.5 ± 0.5°C) and HTO (20.5 ± 0.5°C) Tracers.	20
Table 10	Diffusion Properties of Cobourg Formation Limestone from Bowmanville Determined from Replicate TD Measurements using KI and HTO Tracers.....	23

LIST OF FIGURES

Figure 1 Example of drying curve for determination of saturated surface dry mass M_{sat}2
 Figure 2 Diagram of the diffusion cell used for diffusion experiments by X-ray radiography6
 Figure 3 Images of $\Delta\mu$ differences (colourized) for shale sample DGR2_456.97-PB during a diffusion experiment (t=48 hrs and t=168 hrs) and after the sample was fully saturated with iodide tracer.7
 Figure 4 One-dimensional profiles of $\Delta\mu$ for a shale sample DGR2-456.97-PB obtained from radiography measurements using iodide tracer during a diffusion experiment.....8
 Figure 5 Images of $\Delta\mu$ differences (colourized) for limestone sample DGR2-792.52-NB2 during a diffusion experiment (t=192 hrs and t=267 hrs), and after the sample was fully saturated with iodide tracer.....8
 Figure 6 One-dimensional profiles of $\Delta\mu$ for a limestone sample DGR2-792.52-NB2 obtained from radiography measurements using iodide tracer during a diffusion experiment.....9
 Figure 7 a) Through-diffusion cell (top view), and b) the complete experimental set-up.11
 Figure 8 RGB image showing the presence of anhydrite, dolomite and calcite in the limestone sample DGR2-660.93.14
 Figure 9 Examples of 1D relative iodide tracer concentration profiles (C/C_0) for paired samples of DGR-2 shale (left) and limestone (right) prepared normal (NB) and parallel (PB) to bedding.15
 Figure 10 Images of $\Delta\mu$ distribution for shale sample DGR2-456.97. The images are acquired from the samples after saturation with NaI, and the texture therefore reflects relative spatial variations in porosity.17
 Figure 11 Profiles of ϕ_l for DGR2-456.97-NB and DGR2-456.97-PB.17
 Figure 12 Relationship between ϕ_w and ϕ_l from radiography measurements.....18
 Figure 13 Plots of HTO flux versus time for DRG-2-NB samples obtained from through-diffusion experiments: a) shale samples $C_0 = 5,000$ Bq/mL and b) limestone samples $C_0 = 50,000$ Bq/mL.18
 Figure 14 Plots of iodide flux versus time for DRG-2-NB samples obtained from through-diffusion experiments $C_0 = 1.0$ M NaI: a) shale and b) limestone samples.19
 Figure 15 Plots of cumulative HTO flux by diffusion for DGR-2-NB samples: a) shale samples $C_0 = 5,000$ Bq/mL and b) limestone samples $C_0 = 50,000$ Bq/mL.19
 Figure 16 Plots of cumulative iodide flux by diffusion for DGR-2-NB samples, $C_0 = 1.0$ M NaI: a) shale and b) limestone samples.....20
 Figure 17 Comparison of D_e values obtained from TD experiments with HTO and NaI tracers.21
 Figure 18 Relationship of ϕ_w to ϕ_l and ϕ_{HTO} from TD measurements.....21
 Figure 19 Plots of D_e determined by X-ray radiography and/or TD versus depth (m) from which the rock samples were collected.22

LIST OF APPENDICES

APPENDIX A Photographs of the Core Segments
 APPENDIX B One-Dimensional Diffusion Profiles Determined by X-Ray Radiography for DGR-2 Samples

1 Introduction

Intera Engineering Ltd. has been contracted by the Nuclear Waste Management Organization (NWMO) to implement the Geoscientific Site Characterization Plan (GSCP) for the Bruce nuclear site located near Tiverton, Ontario. The purpose of this site characterization work is to assess the suitability of the Bruce nuclear site to construct a Deep Geologic Repository (DGR) to store low-level and intermediate-level radioactive waste. The GSCP is described by Intera Engineering Ltd., (2006, 2008).

This Technical Report (TR) presents the results from laboratory measurements of diffusion properties of shale and limestone samples from cores OS-1, St. Mary’s Cement Quarry, Bowmanville, Ontario, and from DGR-2, Bruce site, Ontario. Diffusion testing was completed by the University of New Brunswick under contract with Intera Engineering Ltd.

A non-destructive X-ray radiography technique has been developed for the quantitative measurement of diffusion properties of rocks. Diffusion measurements have also been made using a conventional through-diffusion (TD) method as a benchmark for the new technique.

Additional analyses have been conducted in support of diffusion measurements, including water-loss porosity (ϕ_w) by gravimetric methods, mineralogical determinations by Scanning Electron Microscope-Energy Dispersive Spectral (SEM-EDS) analyses, and estimation of the pore-water chemical composition by crush-and-leach. Results of these analyses are also presented in this report.

Work described in this Technical Report was completed in accordance with Test Plan TP-06-12 – Measurement of Diffusion Properties by X-Ray Radiography (Intera Engineering Ltd., 2007), which was prepared following the general requirements of the DGR Project Quality Plan (Intera Engineering Ltd., 2009).

The general procedures for the diffusion measurements are described in Test Plan TP-06-12. Additional details and data from the experiments are recorded in Scientific Notebooks SN-06-12A (L. Cavé) and SN-06-12B (Y. Xiang). The development of the methods and the preliminary results were documented in previous progress reports (Al et al., 2007a; 2007b; 2007c). This report presents the final results of the diffusion work program on DGR-2 samples.

2 Sample Descriptions and Sub-Sampling

Two drill core samples, labelled OS1-044.57 and OS1-075.97 (Table 1), were obtained from borehole OS-1, St. Mary’s Cement Quarry, Bowmanville. They were received in vacuum-sealed foil packaging inside a cooler sent by overnight courier from Intera Engineering Ltd. (Intera). The samples were collected from depths of 44.57 m and 75.97 metres below ground surface (mBGS) measured to the centre of each core segment. The samples were received in good condition with seals intact and were still saturated with their natural pore water when the packaging was opened. The limestone samples are composed mainly of carbonate minerals with minor clay. Sample OS1-044.57 appeared to have a higher content of clay minerals (dark layers) which caused planes of weakness where the core was easily broken.

Table 1 Description of OS-1 Limestone Core Samples Received from Intera

Sample ID	Formation	Description	Date Collected	Length (cm)	Mass (g) Intera	Condition on Arrival
OS1-044.57	Cobourg	limestone	13-Sept-06	12	2254.2	IS intact
OS1-075.97	Cobourg	limestone	13-Sept-06	18	1306.0	IS intact

Note: IS = inner seal on polyethylene bag.

A total of 18 samples were collected from borehole DGR-2 at the Bruce site (Table 2). These samples were shipped to UNB by Intera where they were sub-sampled for a variety of laboratory tests (Table 3).

For the OS-1 and DGR-2 samples, small cylindrical samples (11 mm diameter, 15 to 20 mm length) oriented both parallel and normal to the bedding planes (PB and NB, respectively hereafter) were prepared for the diffusion tests by drilling with a diamond core bit as described in TP-06-12 and SN-06-12A. Cylindrical samples (25.2 mm diameter, 10 mm thickness), oriented with the cylindrical axis normal to bedding, were prepared for the through diffusion tests. The off-cuts from sub-sampling were used for porosity testing.

All samples were cut, and minicores were drilled in water because the severe swelling and cracking encountered with previously archived samples of Queenston shale did not occur with the fresh and preserved cores. This eliminated the need to work with a kerosene cutting fluid. Photographs of the core segments with annotation showing the location of sub-samples are compiled in Appendix A.

3 Methods

3.1 Water-Loss Porosity

Measurements of ϕ_w are used for comparison with tracer-accessible porosity determinations from the radiography and TD experiments. Experimental procedures for the water-loss method were described in detail in TP-06-12 (Intera Engineering Ltd., 2007), and they are consistent with that of Blum (1997) such that the measurements account for the high salinity of the pore water.

Samples from OS-1 and DGR-2 were received saturated with natural pore water. Immediately after sub-sampling, the mass of the saturated sample was determined while the sample was submerged in a brine solution. The beaker of brine was then removed and the mass of the suspended sample was determined repeatedly over time to plot a surface drying curve (Figure 1). The mass of the saturated surface-dry sample was determined at the critical point of slope change (indicating a change from surface evaporation to pore fluid evaporation). Samples were then oven-dried at 105°C and the mass monitored over several weeks. The final dry mass was then recorded when a constant mass was obtained.

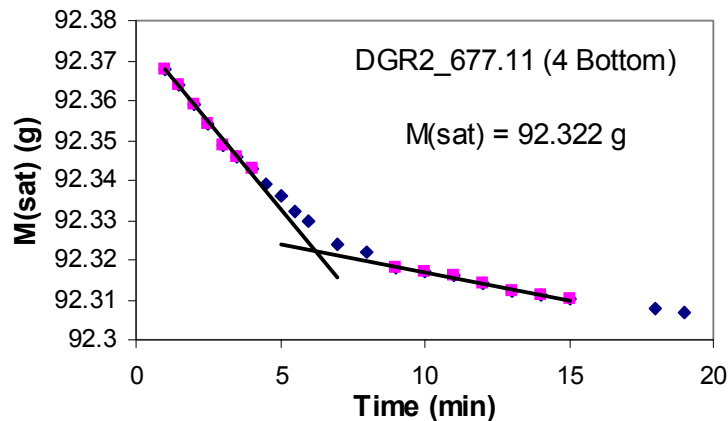


Figure 1 Example of drying curve for determination of saturated surface dry mass M_{sa}

Table 2 Description of DGR-2 Rock Core Samples Received from Intera

Sample ID	Formation	Description	Date Collected	Length (cm)	Mass (g) INTERA	Mass (g) UNB	Condition on Arrival
DGR2-456.97	Queenston	red shale	29-May-07	24	3227.37	3227.2	IS intact
<i>DGR-492.17</i>	<i>Queenston</i>	<i>limestone, resealed</i>	<i>30-May-07</i>	36	>4000	4363.9	<i>OS broken IS not opened</i>
DGR2-517.96	Queenston	red/green shale	30-May-07	22	2725.42	2728.7	OS broken IS intact
DGR2-554.55	Georgian Bay	fissile grey shale	01-Jun-07	20	2336.38	2339.2	Bag torn, IS intact
<i>DGR2-578.56</i>	<i>Georgian Bay</i>	<i>unopened</i>	<i>01-Jun-07</i>	-	3632.8	3632.3	<i>OS intact</i>
DGR2-596.64	Georgian Bay	fissile grey shale, H ₂ S	02-Jun-07	28	3240.12	3239.8	OS broken IS broken
<i>DGR2-614.47</i>	<i>Blue Mountain</i>	<i>unopened</i>	<i>02-Jun-07</i>	-	3507.02	3506.8	<i>OS intact</i>
DGR2-631.22	Blue Mountain	fissile grey shale	03-Jun-07	28	3344.36	3344	OS broken IS intact
<i>DGR2-649.29</i>	<i>Blue Mountain</i>	<i>unopened</i>	<i>03-Jun-07</i>	-	3213.03	3212.5	<i>OS broken</i>
DGR2-660.93	Cobourg	limestone	11-Jun-07	29	3584.73	3584.3	Both bags torn
<i>DGR2-668.19</i>	<i>Cobourg</i>	<i>unopened</i>	<i>11-Jun-07</i>	-	>4000	4250.1	<i>OS intact</i>
DGR2-677.11	Cobourg	limestone	11-Jun-07	31	3864.33	3864.4	OS broken IS intact
DGR2-687.91	Cobourg	limestone (2 textures)	11-Jun-07	41	>4000	5028.5	OS broken IS broken
DGR2-705.68	Sherman Fall	fossiliferous limestone	13-Jun-07	23	2793.28	2793.1	Bag torn, IS broken
DGR2-746.33	Kirkfield	argillaceous limestone	14-Jun-07	24	2982.32	2981.8	Bag torn, IS intact
DGR2-792.52	Gull River	argillaceous limestone	19-Jun-07	34	>4000	4216	OS broken IS intact, wrapped
DGR2-819.52	Gull River	limestone	22-Jun-07	30	3805.25	3804.7	OS broken IS broken, wrapped
<i>DGR2-846.17</i>	<i>Cambrian</i>	<i>unopened</i>	<i>23-Jun-07</i>	-	3308.42	3308	<i>OS broken</i>

NOTES: Depth is measured to the centre of the core segment; OS = outer seal on aluminum foil bag, IS = inner seal on polyethylene bag, wrapped = sample covered in plastic film wrap. Unopened samples shown in italic font have been archived.

Table 3 Sub Samples Cut From DGR-2 Rock Cores

Sample ID	Formation	UNB Rad NB	UNB Rad PB	UNB TD	UNB ϕ_w	UNB TS	UniBern	PSI TD
DGR2-456.97	Queenston	x	X	x	2T, 2B	PB	x	x
DGR2-517.96	Queenston	x	X		2M, 1B	NB	x	
DGR2-554.55	Georgian Bay	x			1T, 2B	NB	x	
DGR2-596.64	Georgian Bay	x	X	x	1T, 2M	PB	x	
DGR2-631.22	Blue Mountain	x		x	2T, 1B	NB	x	
DGR2-660.93	Cobourg	x	X		1M, 2B	NB	x	
DGR2-677.11	Cobourg	x	X	x	2M, 2B	PB	x	x
DGR2-687.91	Cobourg	x	X		2M, 2B	1NB, 1PB	x	
DGR2-705.68	Sherman Fall	x			2T, 1B	NB	x	
DGR2-746.33	Kirkfield			x	1T, 2B	NB	x	
DGR2-792.52	Gull River	x			1M, 2B	NB	x	
DGR2-819.52	Gull River			x	1T, 2B	1NB, 1PB	x	
Total		10	6	6	39	14	12	2

NOTES: NB = long axis normal to bedding; PB = long axis parallel to bedding; Rad = radiography; TD = through diffusion; TS = thin section; T, M, B indicate water-loss porosity (ϕ_w) samples cut from near the top, middle and bottom of each core segment, respectively.

A brine solution containing 4 M NaCl and 0.5 M CaCl₂ was formulated so that its overall salinity is comparable to that of the natural pore water of the samples. The density of this brine solution was determined to be 1.187 g/mL at 24°C. The density of the formulated brine solution (ρ_{brine}) must be taken into account in porosity calculations. To obtain an accurate mass for a dry rock sample, the mass of the salts precipitated from the pore water during drying must be subtracted from mass of the dry sample because the salinity of the natural pore water is high. The modified equations for the determination of porosity and grain density by this method are (Blum P. 1997, SN-06-12B p.14):

$$V_{rock} = \frac{M_{sat} - M_{sub}}{\rho_{brine}} \quad [1]$$

$$V_{voids} = \frac{M_{sat} - M_{dry}}{(1-x)\rho_{brine}} \quad [2]$$

$$\phi_w = \frac{V_{voids}}{V_{rock}} \times 100\% = \frac{M_{sat} - M_{dry}}{(1-x)[M_{sat} - M_{sub}]} \times 100\% \quad [3]$$

$$M_{rock} = M_{dry} - M_{salts} = M_{dry} - (V_{voids} \cdot \rho_{brine} \cdot x) \quad [4]$$

$$\rho_{gr} = \frac{M_{rock}}{V_{rock} - V_{voids}} \quad [5]$$

where: V_{rock} is the calculated volume of the rock, V_{voids} is the calculated volume of the voids, M_{rock} is the calculated mass of the rock, M_{sat} is the mass of the saturated, surface-dry sample weighed in air; M_{sub} is the mass of the saturated sample weighed by suspension when submerged in brine; M_{dry} is the mass of the oven-dried sample (including salts retained in voids) weighed in air; M_{salts} is the mass of salts precipitated from the pore water during drying; ρ_{brine} is the density of the formulated brine solution (assumed to have the same density as the natural pore water); x is the mass fraction of the salts in the natural pore water; and ρ_{gr} is the average grain density of the rock sample.

3.2 Pore Water Composition

Synthetic pore water (SPW) solutions were formulated for use in the diffusion experiments in order to match the composition and ionic strength of the natural pore water, and thereby eliminate the influence of osmotic gradients. A total of 6 samples, representing three different rock types: red shale, grey shale and limestone, were prepared for crush-and-leach determinations of natural pore water compositions.

Samples saturated with natural pore water were first crushed coarsely, and then oven dried at 40°C for 6 days. Crushed samples were milled and sieved to <105 µm particle size then dried again at 40°C to a constant mass. Samples were then weighed into plastic bottles, de-ionized water added, and they were agitated on a rotating or wrist-action shaker for 48 hours. After allowing the solid to settle over night, the supernatant liquid was filtered (0.45 µm) prior to chemical analysis of major cations and anions. Four separate water/rock ratios (1:10, 1:4, 1:2 and 1:1) were used for each sample.

The concentrations of conservative solutes in the pore water were calculated from leach test data using the equation (Koroleva and Mazurek, 2006):

$$C_{pore\ water} = C_{rock} \times \rho_{gr} \times (1 - \phi) / \phi \quad [6]$$

Where $C_{pore\ water}$ is the concentration in mol/L pore water; C_{rock} is the concentration in mol/kg rock sample used for pore water extraction; ρ_{gr} is the grain density (kg/L) obtained from the water-loss porosity determination method; and ϕ is the ion-accessible porosity. The C_{rock} data were obtained from chemical analysis, and ϕ_w data are used to represent the ion-accessible porosity.

PHREEQC modelling simulations using the pitzer.dat database for saline solutions were used to investigate the saturation state of the pore waters with respect to various evaporite minerals. The model was also used to calculate the reduction in the concentration of sulfate required to bring the solutions to saturation with respect to anhydrite

3.3 Diffusion and Porosity Measurements – Radiography

The cylindrical sub-cores (11 mm diameter, 15 to 20 mm length) prepared from core samples were brushed with a thin coat of silicone, enclosed in heat-shrink tubing (3M FP-301) and then attached to the reservoirs of the diffusion cells (Figure 2). The samples were saturated under vacuum for 4 weeks in SPW solution. After saturating the samples, an aluminum disc (11 mm diameter, 3 mm height) was placed on top of each saturated rock cylinder, and a thin aluminum wire was fixed vertically to the side of the shrink tubing. The Al disc is used as an internal standard to correct for inconsistencies in the X-ray source, and the Al wire acts as an alignment guide.

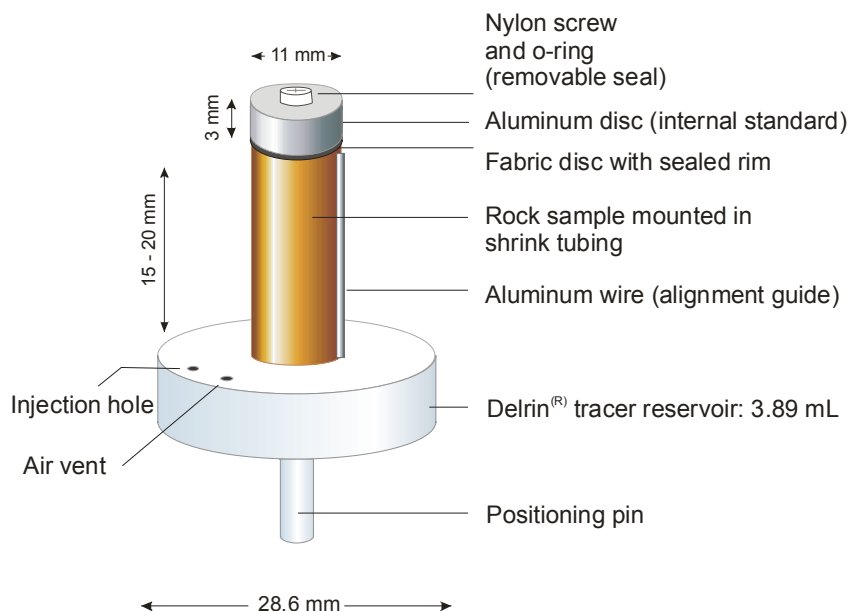


Figure 2 Diagram of the diffusion cell used for diffusion experiments by X-ray radiography

Diffusion experiments were initiated by filling the reservoirs of the diffusion cells with 1.0 M NaI tracer solution and covering the injection holes with electrical tape. Reference radiographs were collected immediately after tracer solution was injected. Samples were stored at 22 ± 1 °C in a closed container with an open dish of water to maintain high humidity and prevent evaporative drying of the samples. Time-series radiographs were collected at intervals of 2-7 days, starting 48 hrs after the tracer was added, and continued until iodide breakthrough occurred at the top end of the samples (up to 504 hrs). During this time the tracer solutions in the reservoirs were refreshed periodically. After iodide break through, the samples were saturated with NaI tracer from both ends by removing the nylon screw caps in the aluminum discs (Figure 2) and submerging in the 1.0 M NaI tracer solution. The progress of saturation is monitored by X-ray radiography until no changes are observed in X-ray attenuation between consecutive images. A time period of 3 to 4 weeks was required to saturate the DGR2 samples, after which time the final radiographs for the tracer-saturated samples were collected.

All data were collected as digital radiographs (16 bit greyscale TIFF files) using a Skyscan 1072 desktop microCT instrument. The instrumental settings used for all DGR-2 data acquisition are shown in Table 4.

Table 4 X-Ray Radiography Data Acquisition Parameters for OS-1 and DGR-2 Samples

Parameter	Setting	Parameter	Setting
Height	4.5 mm	Source energy	90 kV
Magnification	14 times	Source current	110 μ A
Resolution	18.68 μ m/pixel	Source filter	1 mm Al
Alignment	Al wire on right hand side	Acquisition time	9968 ms
Flat field correction	On	Frames averaged	4

The principle of the X-ray radiography technique, and the data processing procedures, were described in TP-06-12. Briefly, data are collected in the form of two-dimensional (2D) digital radiographs where the greyscale value at each pixel is a function of the X-ray intensity measured by the detector, which represents the difference between the X-ray source intensity and the X-ray absorption in the sample:

$$I = I_0 e^{-\mu d} \tag{7}$$

where I is the measured X-ray intensity (greyscale value); I_0 is the source X-ray intensity; μ is the X-ray attenuation coefficient; and d is the thickness of the sample. Because of the cylindrical geometry of the sample, the X-ray path length through the sample varies from zero at the edges to the sample diameter (11 mm) at the centre. Intensity measurements from 2D radiographs are integrated horizontally across the width of the sample thereby producing 1D profiles of X-ray intensity vs. distance along the axis of the sample and removing the effects of lateral thickness variation.

Using an approach in which the difference in X-ray attenuation between a reference image (Time = 0) and a time-series image (Time = t) is calculated as:

$$\Delta\mu d = [\ln(I_{ref}) - \ln(I_t)] \tag{8}$$

The background X-ray absorption due to the rock matrix is removed and only the net X-ray absorption due to the presence of the tracer (iodide) is recorded. The thickness, d , of the samples is constant and $\Delta\mu d$ is represented as $\Delta\mu$.

As an example, Figure 3 presents images of $\Delta\mu$ obtained from a diffusion experiment with a shale sample (DGR2_456.97_PB) by subtracting the log-transformed time-series radiographs from the log-transformed reference radiograph ($\ln(I_{ref}) - \ln(I_t)$ where $t = 48$ and 168 hrs) and correcting for the cylindrical geometry. In general, the pixel brightness is proportional to iodide concentration, and it is evident that iodide concentrations increase with time from bottom to top. The digital radiograph data are reduced to 1D $\Delta\mu$ profiles in Figure 4.

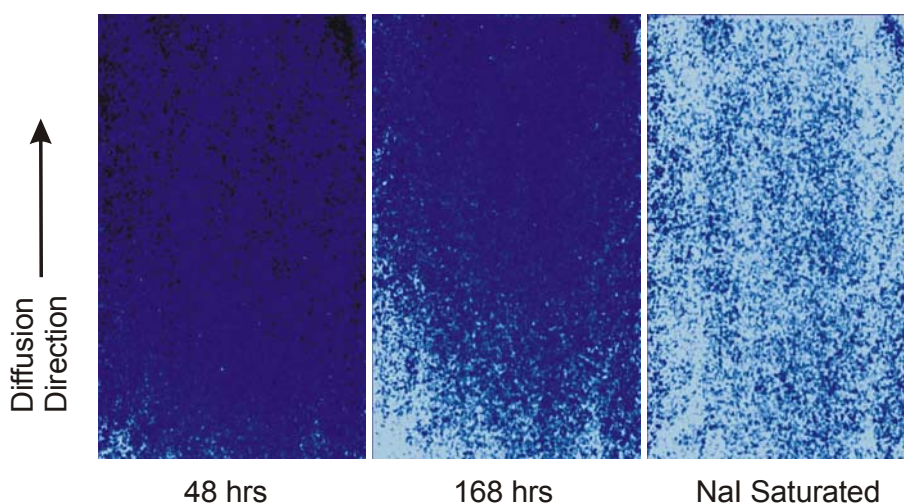


Figure 3 Images of $\Delta\mu$ differences (colourized) for shale sample DGR2-456.97-PB during a diffusion experiment ($t=48$ hrs and $t=168$ hrs) and after the sample was fully saturated with iodide tracer.

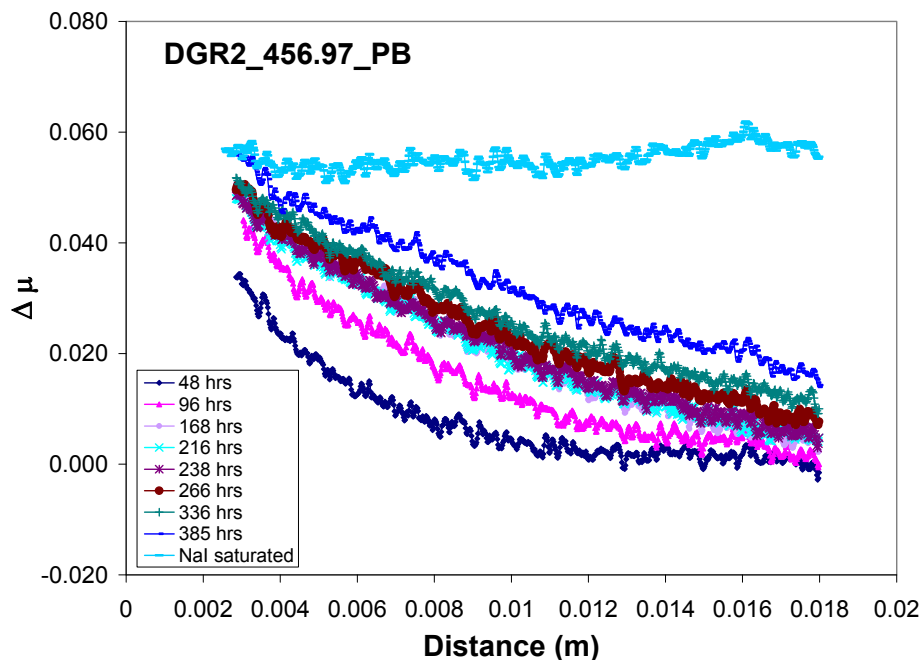


Figure 4 One-dimensional profiles of $\Delta\mu$ for a shale sample DGR2-456.97-PB obtained from radiography measurements using iodide tracer during a diffusion experiment.

A similar example for limestone is presented in Figure 5, however, the ratio of signal-to-noise for the radiography measurements is low owing to the lower porosity of the limestone. Profiles of $\Delta\mu$ are presented in Figure 6 for the corresponding limestone sample.

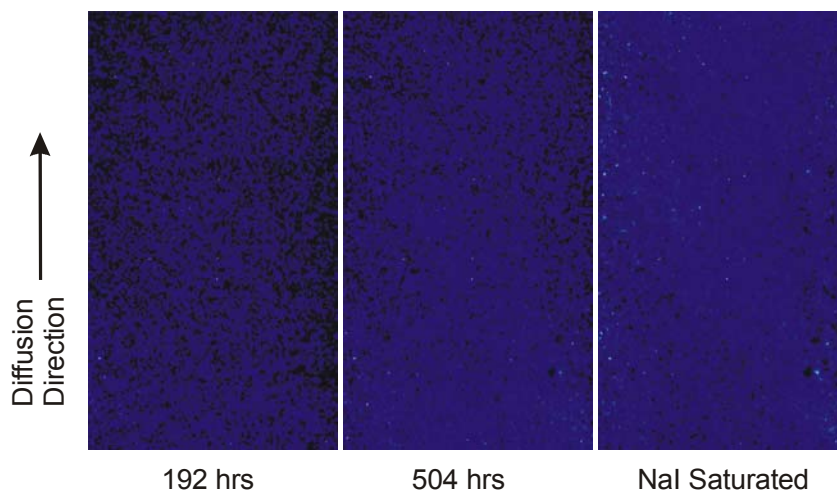


Figure 5 Images of $\Delta\mu$ differences (coloured) for limestone sample DGR2-792.52-NB2 during a diffusion experiment ($t=192$ hrs and $t=267$ hrs), and after the sample was fully saturated with iodide tracer.

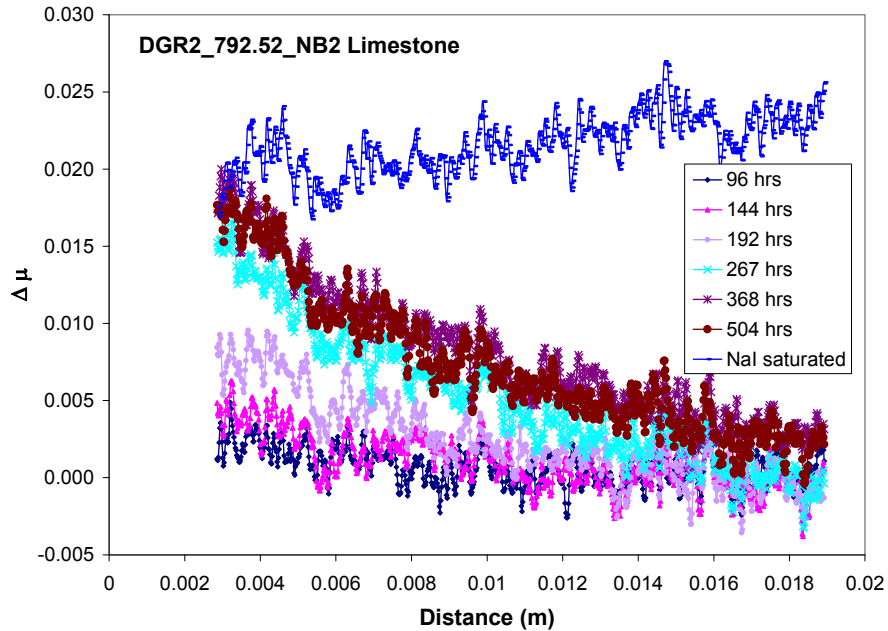


Figure 6 One-dimensional profiles of $\Delta\mu$ for a limestone sample DGR2-792.52-NB2 obtained from radiography measurements using iodide tracer during a diffusion experiment.

The numerical value of $\Delta\mu$ is a function of the concentration (C) of the iodide tracer present in the pores. As described in test plan TP-06-12 (Intera Engineering Ltd., 2007a), two approaches have been used to transform $\Delta\mu$ in time-series data to relative concentration profiles (C/C_0). First is a relative approach, similar to that presented by Tidwell et al (2000) in which:

$$\frac{C}{C_0} = \frac{\Delta\mu_t}{\Delta\mu_{sat}} \quad [9]$$

where $\Delta\mu_{sat}$ is obtained from the tracer-saturated sample. This relative approach does not require knowledge of the porosity, but it is not accurate when low porosity values ($< 3\%$) cause low signal/noise ratios. An alternate approach is to use a calibration curve for C versus $\Delta\mu$ to calculate C at all points in the sample. The correlation between C and $\Delta\mu$ is calibrated (Al et al., 2007a) using a series of standard solutions of NaI in SPW matrix in glass vials (11 mm diameter).

The calibrated approach requires knowledge of the porosity, and most applications of this approach have utilized ϕ_w values determined independently with the gravimetric technique. The ϕ_w values are not an ideal choice because they represent bulk values, and because they do not take into account differences in ϕ_w and ϕ_l . For these reasons, the calibrated approach is reserved for use when low signal/noise ratio (low porosity) prevents the use of the relative approach. In this case, ϕ_w is used as a first approximation, but it is commonly necessary to adjust the porosity term to lower values to obtain a realistic concentration profile (such that $C/C_0 = 1$ at influx boundary). This reduction of the porosity term should be justified because it is known that due to ion size effects ϕ_l may be lower than ϕ_w for many porous media samples.

When a sample is saturated with a constant concentration of iodide tracer the $\Delta\mu$ values are proportional to the iodide-accessible porosity (ϕ_l), and the calibration data are used to obtain quantitative profiles of ϕ_l :

$$\phi_I = \frac{\Delta\mu_{sat}}{\Delta\mu_{std}} \quad [10]$$

where, $\Delta\mu_{std}$ is the X-ray attenuation difference between standards solutions prepared from 1 mol/L NaI and SPW.

Diffusion coefficients may be obtained by fitting experimental profiles of iodide concentrations with theoretical profiles obtained from an analytical solution for Fick's Law (Intera Engineering Ltd., 2007):

$$\frac{C}{C_0} = \text{erfc} \left[\frac{x}{2\sqrt{D_p t}} \right] \quad [11]$$

where C is the measured concentration of the tracer at position x (m); C_0 is the constant concentration of the tracer at the influx boundary; t is the time (s) since the start of diffusion; and D_p is the pore-water diffusion coefficient (m^2/s).

Experimental data are visually fitted with the theoretical curves using an iterative curve-matching process that relies on trial-and-error estimates of D_p . In order to provide ease of comparison with results of TD experiments, effective diffusion coefficients, D_e (m^2/s), may be estimated from D_p and the average iodide-accessible porosity values (ϕ_I):

$$D_e = \phi_I D_p \quad [12]$$

3.4 Diffusion Measurements – Through Diffusion

The experimental procedures for TD measurements were described previously by Al et. al., (2007b), but some modifications have been made to the cell design (Fig. 7). The cylindrical sub-core (25.2 mm diameter, 10 mm height) was positioned inside flexible vinyl tubing (25.4 mm ID, 3.3 mm wall thickness), a heat-shrink clamp (PowerGrip, McMaster-Carr) was placed around the tubing, and a pair of steel gear clamps were placed around the heat-shrink clamp. Porous stainless steel discs (100 μm average pore diameter, Mott Industrial, USA) was placed inside the tubing and clamp assembly, one disc against each face of the sample. A delrin plug, with ports that connect to the solution reservoirs, was positioned against the porous disc inside each end of the tubing and clamp assembly. After assembling the cell in this way, the heat-shrink clamp and the gear clamps were tightened around the circumference of the sample.

To ensure that leakage does not occur between the sample and the tubing, each cell was tested by applying fluid pressure to the ports on one side using a syringe filled with synthetic pore water (SPW). After passing the leakage test, the cell was attached to the reservoirs and a peristaltic pump (205U Watson Marlow or Ecoline VC-MS/CAB-6, Ismatec) via fluoropolymer tubing (Figure 7b). The speed of the pump was adjusted to 28 mL/hr. The experiment was set up so that the direction of tracer flux or diffusion was from bottom to top. All the joints of the cells were airtight and the cells were maintained in the open atmosphere in the laboratories at $20.5 \pm 0.5^\circ\text{C}$ for HTO and $23.5 \pm 0.5^\circ\text{C}$ for NaI diffusion experiments.

Although samples are prepared from cores that were received saturated with natural pore water, some drying may occur at the outer surfaces during preparation and loading of the diffusion cells. Samples were re-saturated by circulating SPW solution in both reservoirs for three weeks prior to starting the experiments. Following the

saturation period, SPW in the tracer reservoirs was replaced by tritiated water (HTO) (5,000 Bq/mL for shale and 50,000 Bq/mL for limestone) prepared in SPW matrix. The low concentration reservoirs contained a known volume of SPW solution. The quantity of radioactive ^3H (in Bq) that diffused through the samples was determined by liquid scintillation counting (LS 6000 Series, Beckman, BCS scintillation cocktail, GE Healthcare). Data were collected in time intervals of 3-4 days. Fresh SPW solutions of known volumes were replaced in the low concentration reservoirs after each measurement. All diffusion cells were maintained in a fume hood at $20.5 \pm 0.5^\circ\text{C}$.

Following the HTO diffusion experiments, HTO was removed from the samples by circulating the SPW solutions in both reservoirs until no ^3H activity was detected. The iodide diffusion experiments were then started by replacing SPW in the tracer reservoirs with 1.0 M NaI solution prepared in a SPW matrix. The quantity of the iodide tracer (in mmol/mL) that diffused to the low concentration reservoirs was determined by an iodide ion selective electrode (combined ISE, London Scientific Limited) in time intervals of 2-3 days. Fresh SPW solutions of known volumes were replaced in the low concentration reservoirs after each measurement. The diffusion cells were maintained at $23.5 \pm 0.5^\circ\text{C}$.

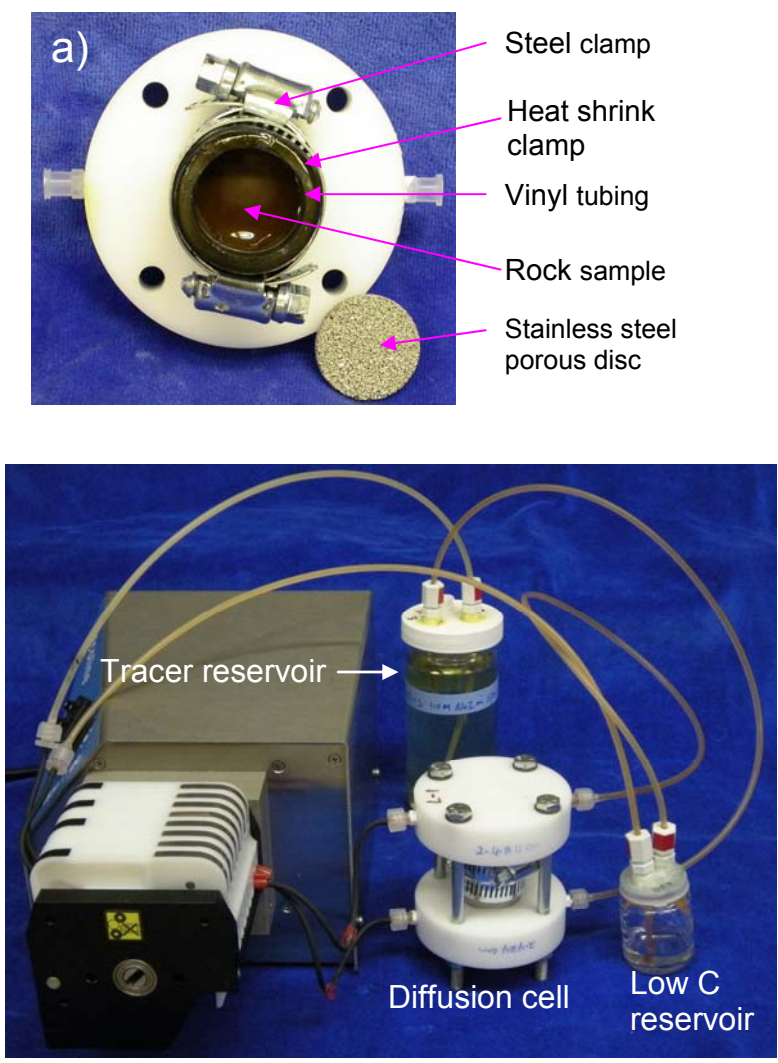


Figure 7 a) Through-diffusion cell (top view), and b) the complete experimental set-up.

4 Results and Discussion

4.1 Water-Loss Porosity

Results of the water-loss porosity measurements for OS-1 and DGR-2 samples are presented in Table 5. Multiple samples were prepared and measured for heterogeneous lithologies. A narrow range of porosity, from 7.5 to 10% has been determined for DGR-2 shales. DGR-2 limestone samples have much lower porosity, ranging from 0.4 to 2.3%.

Table 5 Water Loss Porosity and Grain Density

Sample	Formation	Sub-Sample	Water-Loss Porosity (ϕ_w)	Mean ϕ_w \pm s.d.	Grain Density (ρ_{gr})	Mean ρ_{gr}
OS1-044.57	Cobourg limestone - Bowmanville	1	5.28	4.45 \pm 0.55	2.73	2.72
		2	4.15		2.72	
		3	4.17		2.72	
		4	4.20		2.72	
OS1-075.97	Cobourg limestone - Bowmanville	1	1.98	1.65 \pm 0.28	2.72	2.72
		2	1.58		2.71	
		3	1.30		2.72	
		4	1.73		2.71	
DGR2-456.97	Queenston red shale	1T	8.56	9.04 \pm 0.55	2.80	2.80
		3T	8.58		2.81	
		2B	9.39		2.80	
		4B	9.63		2.81	
DGR2-517.96	Queenston red shale	1M	7.88	7.80 \pm 0.30	2.77	2.77
		3M	8.05		2.78	
		2B	7.47		2.77	
DGR2-554.55	Georgian Bay grey shale	2T	9.11	9.47 \pm 0.44	2.80	2.79
		1B	9.34		2.78	
		3B	9.97		2.80	
DGR2-596.64	Georgian Bay grey shale	2T	8.64	8.25 \pm 0.42	2.79	2.79
		1M	8.29		2.79	
		3M	7.81		2.79	
DGR2-631.22	Blue Mountain grey shale	1T	8.43	8.66 \pm 0.20	2.77	2.78
		3T	8.79		2.77	
		2B	8.76		2.79	
DGR2-660.93	Cobourg limestone	1M	0.80	0.94 \pm 0.13	2.71	2.71
		2B	1.06		2.71	
		3B	0.97		2.71	
DGR2-677.11	Cobourg limestone	1M	2.17	2.12 \pm 0.06	2.72	2.71
		2M	2.04		2.72	
		3B	2.17		2.71	
		4B	2.10		2.71	
DGR2-687.91	Cobourg limestone	2M	2.16	2.15	2.72	2.72
		4M	2.13		2.72	
		1B	0.38	0.38	2.71	
		3B	0.38		2.71	
DGR2-705.68	Sherman Fall limestone	1T	0.45	0.53 \pm 0.11	2.67	2.69
		3T	0.61		2.71	
DGR2-746.33	Kirkfield limestone	3T	2.27	2.27	2.71	2.71
		1B	0.52		2.71	
		2B	0.46		2.71	
DGR2-792.52	Gull River limestone	2M	1.59	1.51 \pm 0.08	2.72	2.72
		1B	1.42		2.72	
		3B	1.52		2.72	
DGR2-819.52	Gull River limestone	2T	1.63	1.43 \pm 0.21	2.78	2.78
		1B	1.42		2.79	
		3B	1.22		2.77	

NOTE: T, M, B = sample taken from the top, middle or bottom of the core segment, respectively.

4.2 Pore Water Composition

The results from the crush-leach data are presented in Table 6. Plots of ion concentrations versus water/rock ratio (not shown) provide linear profiles for sodium, chloride and potassium as well as most of the calcium and magnesium data, suggesting that these ions are not affected by dissolution of salts during the leach process. Non-linearity was observed for calcium in DGR2-456.97 red shale, magnesium in DGR2-631.22 grey shale and all of the sulfate data, suggesting that mineral dissolution reactions, in addition to pore-water dilution, may control the calcium and sulphate concentrations. In particular, it is suspected that anhydrite dissolution may add to the calcium and sulfate concentrations. Anhydrite was observed in thin sections for both shale and limestone rock types (Figure 8).

Table 6 Pore Water Composition Data

Sample	DGR2-456.97	DGR2-517.96	DGR2-596.647	DGR2-631.22	DGR2-677.11	DGR2-746.33
Formation	Queenston	Queenston	Georgian Bay	Blue Mountain	Cobourg	Kirkfield
Rock type	red shale	red shale	grey shale	grey shale	limestone	limestone
Grain density	2.80	2.77	2.79	2.78	2.71	2.71
Porosity ϕ	0.090	0.078	0.083	0.087	0.021	0.023
PORE WATER CONCENTRATIONS (mol/L)						
Na ⁺	1.475	4.116	2.591	2.380	1.197	2.004
K ⁺	0.484	0.475	0.539	0.523	0.447	0.465
Ca ²⁺	1.301	1.057	1.236	1.063	0.376	0.486
Mg ²⁺	0.236	0.291	0.250	0.217	0.175	0.191
Sr ²⁺	0.0081	0.0097	0.0146	0.0127	0.0062	0.0057
SUM Cations	5.050	7.307	6.132	5.487	2.759	3.834
Cl ⁻	3.996	6.841	5.996	5.331	2.399	3.571
Br ⁻	0.021	0.022	0.029	0.025	0.009	0.011
SO ₄ ²⁻	0.415	0.165	0.065	0.049	0.105	0.110
SUM Anions	-4.826	-7.172	-6.127	-5.429	-2.608	-3.790
Ionic strength	6.90	8.76	7.70	6.80	3.35	4.60
BALANCE	2.26%	0.93%	0.04%	0.53%	2.80%	0.57%
Density	1.148	1.244	1.216	1.194	1.090	1.133
kg H ₂ O / L	0.854	0.820	0.858	0.874	0.930	0.906
SATURATION INDICES FROM SPECIATED PHREEQC-PITZER MODEL						
si_Anhydrite	2.06	2.24	1.62	1.30	0.82	1.07
si_Celestite	2.06	2.35	1.84	1.52	1.25	1.32
si_Gypsum	2.09	2.05	1.54	1.27	0.95	1.15
si_Halite	-0.63	0.46	-0.01	-0.24	-1.34	-0.80
si_Sylvite	-0.73	-0.33	-0.44	-0.58	-1.23	-0.97

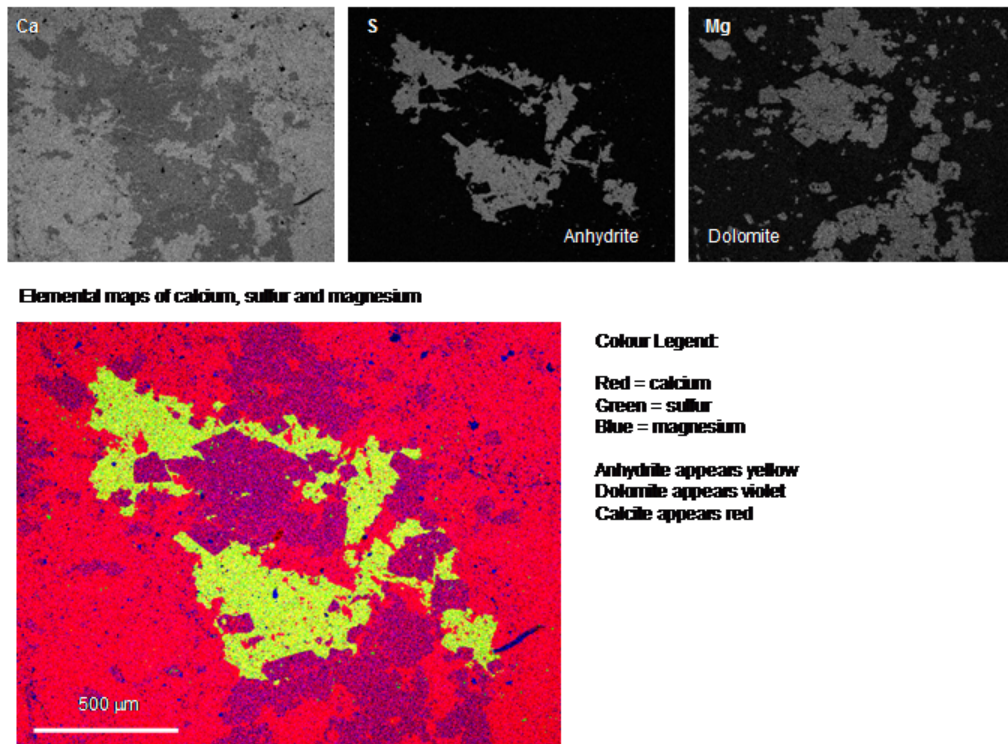


Figure 8 RGB image showing the presence of anhydrite, dolomite and calcite in the limestone sample DGR2-660.93.

The natural pore water compositions suggest that, for the purposes of diffusion measurements, the data can be considered in terms of two separate pore-water compositions, one for shales and a second for limestones. The Na:Ca ratios are quite different in the DGR-2 samples compared to older archived samples (Hobbs et al., 2008). The SPW composition for diffusion experiments with shales was formulated to have a composition close to that of DGR2-596.64, while the SPW composition for diffusion experiments with limestones is based on the natural pore-water composition of DGR2-746.33. The SPW solution compositions that are in use for diffusion experiments are given in Table 7.

Table 7 SPW and Iodide-Tracer Solution Compositions for Diffusion Experiments.

	Shale SPW		Shale Tracer		Limestone SPW		Limestone Tracer	
	mol/L	g/L	mol/L	g/L	mol/L	g/L	mol/L	g/L
NaCl	2.40	140.263	1.40	81.820	2.00	116.886	1.00	58.443
KCl	0.50	37.276	0.50	37.276	0.45	33.548	0.45	33.548
CaCl ₂ (2H ₂ O)	1.20	176.416	1.20	176.416	0.48	70.567	0.48	70.567
MgCl ₂ (6H ₂ O)	0.25	50.825	0.25	50.825	0.20	40.660	0.20	40.660
CaSO ₄	0.001	0.136	0.001	0.136	0.005	0.681	0.01	0.681
Nal	0.00	0.000	1.00	149.890	0.00	0.000	1.00	149.890
Density (calc)	1.210				1.190			
Saturation Indices								
Anhydrite	-0.26				-0.23			
Gypsum	-0.31				-0.16			
Halite	-0.12				-0.77			
Sylvite	-0.53				-0.95			

4.3 Diffusion and Porosity Measurements – Radiography

The pore-water diffusion coefficients (D_p) for 12 of the DGR2 samples range from 1.5×10^{-11} to 8.5×10^{-11} (Figure 9, Table 8 and Appendix B). The D_p data for 4 limestone samples are not reported due to the low signal to noise ratios. The greater variability in effective diffusion coefficients (D_e ; the product of D_p and ϕ_i), particularly between shales and limestones, can be attributed to differences in ϕ_i . The iodide-accessible porosity data for limestones reported here are only estimates. As noted in Section 3.3, the low porosity of limestone samples presents a challenge for accurate measurements.

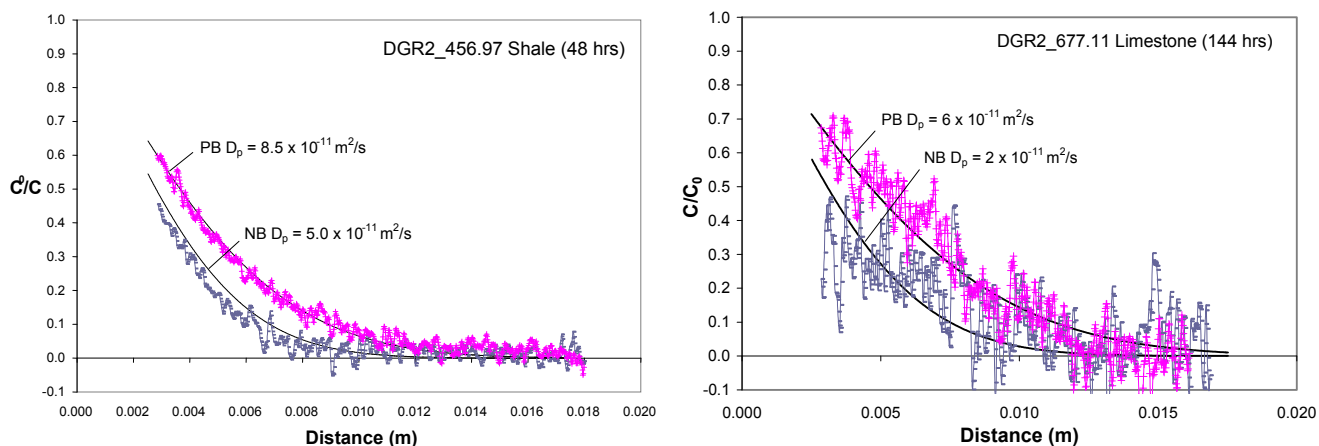


Figure 9 Examples of 1D relative iodide tracer concentration profiles (C/C_0) for paired samples of DGR-2 shale (left) and limestone (right) prepared normal (NB) and parallel (PB) to bedding.

Table 8 Diffusion-Coefficient and ϕ_i Data from X-Ray Radiography (22±1°C).

Sample	Formation	ϕ_w^a	Radiography		
			D_p (m ² /s)	D_e (m ² /s)	ϕ_i
OS1-044NB	Cobourg	0.045	6.91×10^{-11}	3.8×10^{-12}	0.055 ^c
OS1-044PB	Cobourg	0.045	5.11×10^{-11}	2.3×10^{-12}	0.045 ^c
OS1-044PB-2	Cobourg	0.045	5.00×10^{-11}	2.0×10^{-12}	0.040 ^c
OS1-075NB	Cobourg	0.017	6.00×10^{-11}	1.8×10^{-12}	0.030 ^c
OS1-075NB-2	Cobourg	0.017	3.78×10^{-11}	1.7×10^{-12}	0.045 ^c
OS1-075PB-2	Cobourg	0.017	7.22×10^{-11}	2.6×10^{-12}	0.036 ^c
OS1-075PB-3	Cobourg	0.017	6.46×10^{-11}	3.1×10^{-12}	0.048 ^c
DGR2-456.97_NB	Queenston	0.090	5.0×10^{-11}	2.0×10^{-12}	0.040 ^b
DGR2-456.97_PB	Queenston	0.090	8.5×10^{-11}	4.0×10^{-12}	0.047 ^b
DGR2-517.96_NB	Queenston	0.078	4.0×10^{-11}	1.5×10^{-12}	0.037 ^b
DGR2-517.96_PB	Queenston	0.078	7.5×10^{-11}	2.5×10^{-12}	0.035 ^b
DGR2-554.55_NB	Georgian Bay	0.095	2.3×10^{-11}	1.0×10^{-12}	0.044 ^b
DGR2-596.64_NB	Georgian Bay	0.082	3.5×10^{-11}	1.4×10^{-12}	0.039 ^b
DGR2-596.64_PB	Georgian Bay	0.082	7.5×10^{-11}	4.9×10^{-12}	0.067 ^b
DGR2-631.22_NB	Blue Mountain	0.087	1.5×10^{-11}	7.7×10^{-13}	0.051 ^b
DGR2-660.93_NB	Cobourg	0.009	2×10^{-11}	2×10^{-13}	0.009 ^c
DGR2-660.93_PB	Cobourg	0.009	Low S/N	Low S/N	0.009 ^c
DGR2-677.11_NB	Cobourg	0.021	2×10^{-11}	2×10^{-13}	0.01 ^c
DGR2-677.11_PB	Cobourg	0.021	6×10^{-11}	9×10^{-13}	0.015 ^b
DGR2-687.91_NB2	Cobourg	0.013	Low S/N	Low S/N	0.01 ^c
DGR2-687.91_PB2	Cobourg	0.013	Low S/N	Low S/N	0.01 ^c
DGR2-705.68_NB2	Sherman Fall	0.005	Low S/N	Low S/N	0.01 ^c
DGR2-792.52_NB2	Gull River	0.015	3×10^{-11}	5×10^{-13}	0.015 ^b

Notes: ^a average values; ^b determined from iodide-saturated sample; ^c estimated from diffusion profiles by adjusting ϕ_i such that $C/C_0 = 1.0$ at influx boundary; S/N = signal to noise ratio

For the three paired shale samples tested, D_p values determined parallel to bedding are larger than those obtained normal to bedding by a factor ranging from 1.7 to 2.1. A similar anisotropic effect was observed from the one paired limestone sample (DGR2-677.11) where the D_p value parallel to bedding is larger by a factor of three. Visual evidence of anisotropy is presented in $\Delta\mu$ images from samples of Queenston shale (DGR2-456.97; Figure 10). These images reflect the relative distribution of ϕ_i . The average ϕ_i values in these samples were similar (0.040 and 0.047; Table 8), however the alignment of porosity in the direction of diffusion for the sample prepared parallel to bedding suggests a more efficient diffusion path may be available in that direction. Spatial variations in ϕ_i are also illustrated by the 1D profiles presented in Figure 11.

A comparison of the measured values for ϕ_w and ϕ_i (Figure 12) indicates that the values of ϕ_i are consistently lower than ϕ_w for the shale samples. This relationship is consistent with solute-specific variations in porosity that are commonly attributed to ion exclusion effects in the porous medium due to variations in ion size (van Loon et al., 2007).

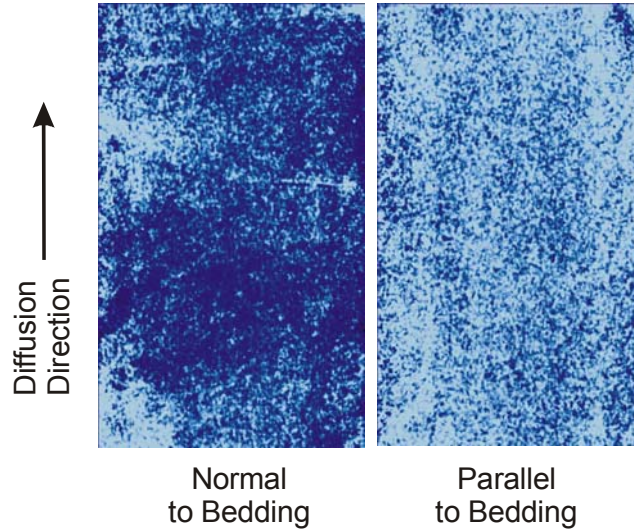


Figure 10 Images of $\Delta\mu$ distribution for shale sample DGR2-456.97. The images are acquired from the samples after saturation with NaI, and the texture therefore reflects relative spatial variations in porosity.

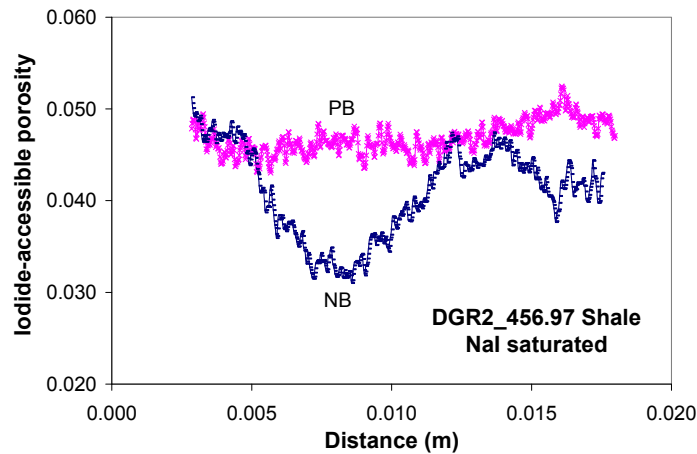


Figure 11 Profiles of ϕ_1 for DGR2-456.97-NB and DGR2-456.97-PB.

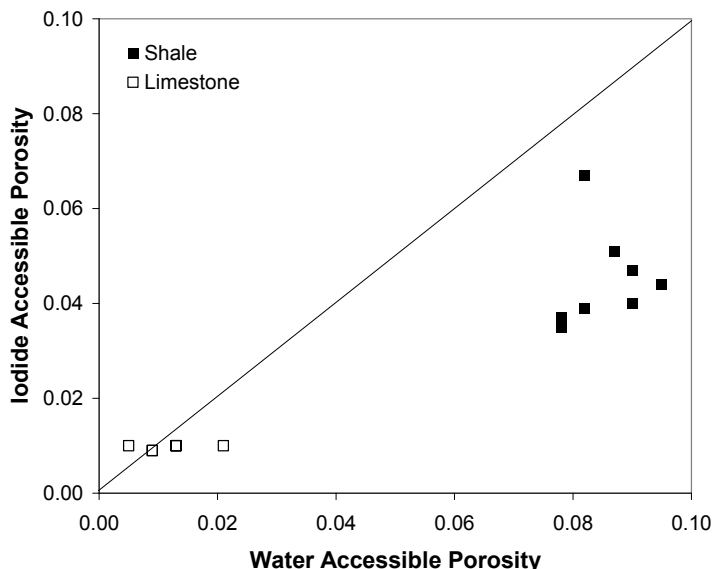


Figure 12 Relationship between ϕ_w and ϕ_i from radiography measurements.

4.4 Diffusion Measurements – Through Diffusion

Through-diffusion (TD) data for six samples (Table 9) were obtained using the method of van Loon et al. (2003) with 1.0 M NaI and tritiated-water (HTO) tracers. The flux of tracer ($\text{Bq}/\text{m}^2/\text{day}$ for HTO and $\text{mmol}/\text{m}^2/\text{day}$ for iodide), and the total accumulated tracer that diffused through the sample Q_t (Bq for HTO and mmol for iodide) are plotted as a function of time (Figures 13-16). Beyond the time to reach steady-state, as represented by constant flux values in Figures 13 and 14, linear regression analysis of Q_t vs. time (Figures 15 and 16) provides values for the effective diffusion coefficient (D_e) and the tracer-accessible porosity (α) from the slope and intercept, respectively.

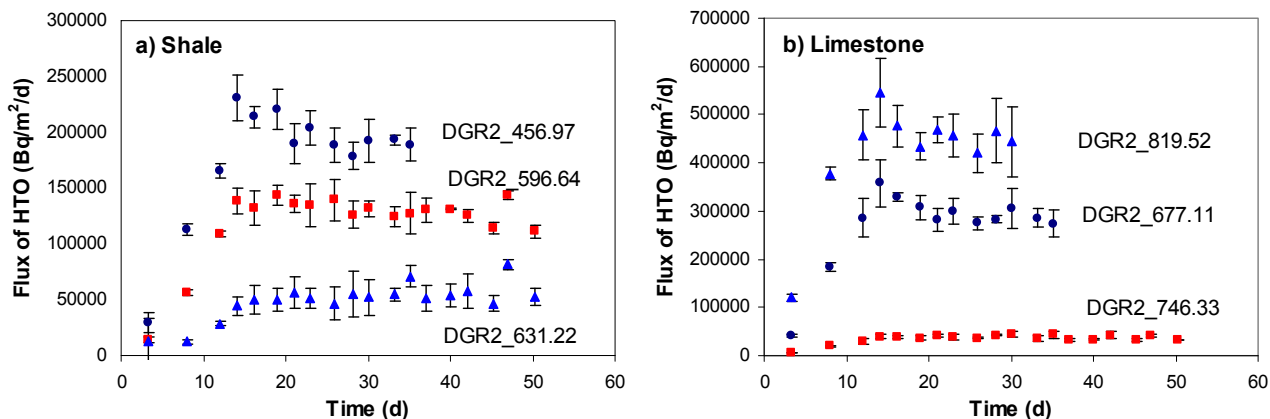


Figure 13 Plots of HTO flux versus time for DRG-2-NB samples obtained from through-diffusion experiments: a) shale samples $C_0 = 5,000 \text{ Bq}/\text{mL}$ and b) limestone samples $C_0 = 50,000 \text{ Bq}/\text{mL}$.

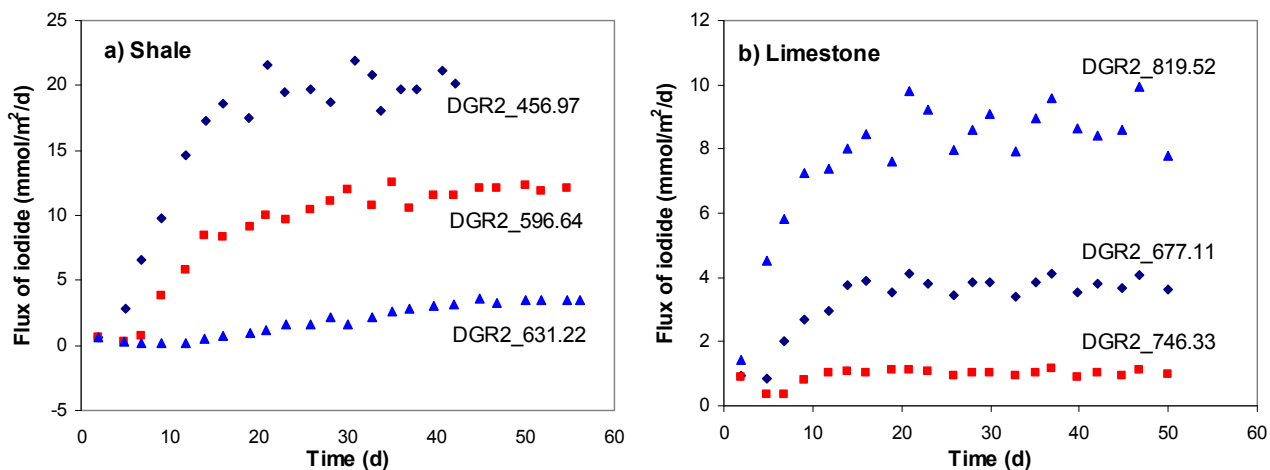


Figure 14 Plots of iodide flux versus time for DRG-2-NB samples obtained from through-diffusion experiments $C_0 = 1.0 \text{ M NaI}$: a) shale and b) limestone samples.

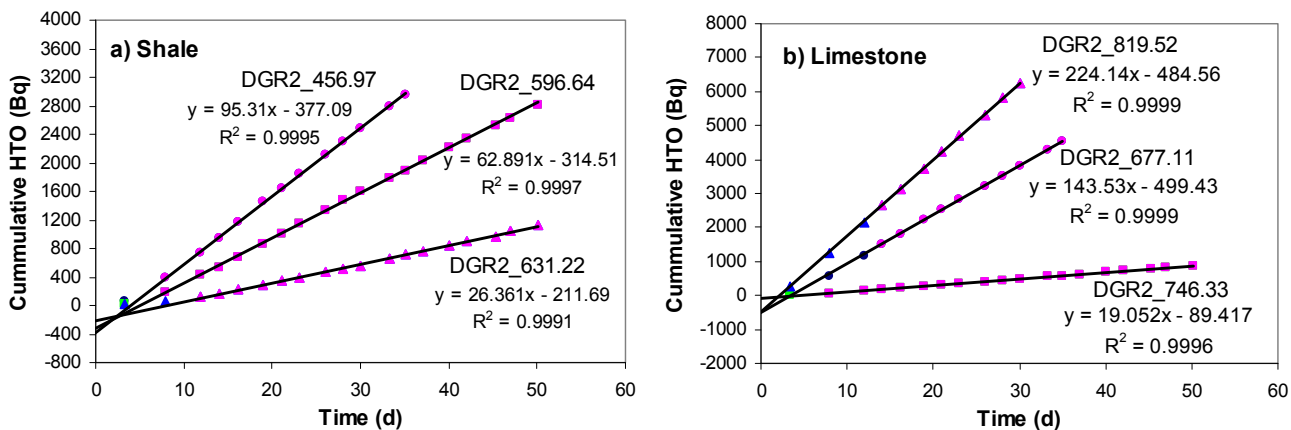


Figure 15 Plots of cumulative HTO flux by diffusion for DGR-2-NB samples: a) shale samples $C_0 = 5,000 \text{ Bq/mL}$ and b) limestone samples $C_0 = 50,000 \text{ Bq/mL}$.

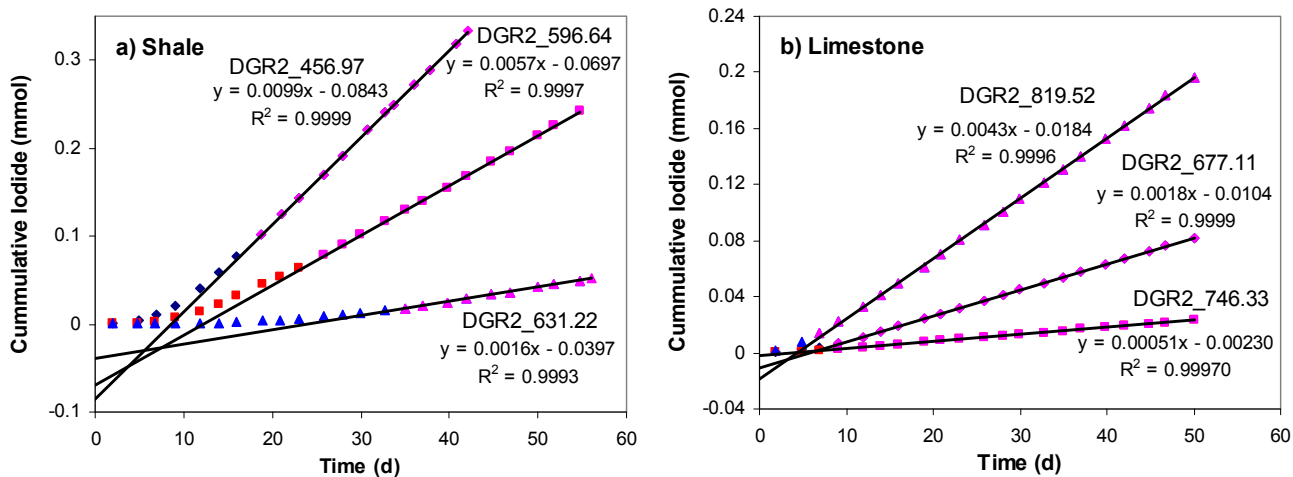


Figure 16 Plots of cumulative iodide flux by diffusion for DGR-2-NB samples, $C_0 = 1.0 \text{ M NaI}$: a) shale and b) limestone samples.

Consistent with an anion exclusion model, the D_e values for shale samples determined from the HTO tracer are greater by a factor of two than those from iodide (Figure 17; Table 9). As might be expected for rock samples with low clay content, the tracer-specific difference is not evident for D_e values from the limestone samples. With the exception of one sample (DGR2-631.22), comparison of the tracer-accessible porosities (α) determined by TD, with the corresponding ϕ_w values (Figure 18), does not indicate solute-specific differences in porosity. This observation is inconsistent with the differences between ϕ_w determined gravimetrically and ϕ_l determined by radiography; however, it is known that TD is not a sensitive method for determination of tracer-accessible porosity (van Loon et al., 2003). Consequently the tracer-accessible porosity values determined from TD testing should be interpreted with caution.

Table 9 Diffusion Coefficient Data and Tracer-Accessible Porosity for DGR-2 Samples Determined Normal to Bedding by TD using 1.0 M NaI ($23.5 \pm 0.5^\circ\text{C}$) and HTO ($20.5 \pm 0.5^\circ\text{C}$) Tracers.

Sample	Formation	ϕ_w^a	Iodide tracer		HTO tracer ^c	
			$D_e \text{ (m}^2\text{/s)}$	α^b	$D_e \text{ (m}^2\text{/s)}$	α^b
DGR2-456.97	Queenston	0.090	2.6×10^{-12}	0.094	4.8×10^{-12}	0.082
DGR2-596.64	Georgian Bay	0.082	1.4×10^{-12}	0.080	3.3×10^{-12}	0.076
DGR2-631.22	Blue Mountain	0.087	4.1×10^{-13}	0.045	1.4×10^{-12}	0.048
DGR2-677.11	Cobourg	0.021	4.5×10^{-13}	0.012	7.8×10^{-13}	0.012
DGR2-746.33	Kirkfield	0.005	1.3×10^{-13}	0.0026	1.0×10^{-13}	0.0022
DGR2-819.52	Gull River	0.015	9.3×10^{-13}	0.023	1.2×10^{-12}	0.012

Notes: ^a average values; ^b tracer-accessible porosity; ^c $C_0 = 5,000 \text{ Bq/mL}$ for shale and $C_0 = 50,000 \text{ Bq/mL}$ for limestone

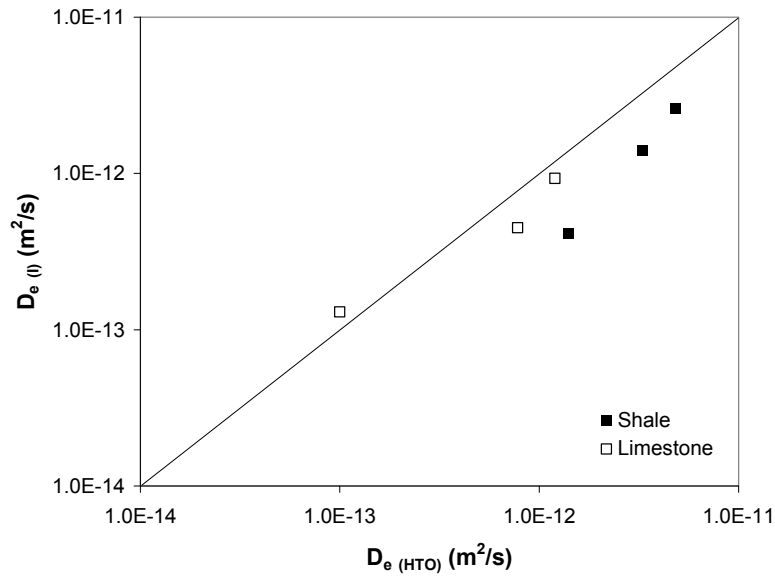


Figure 17 Comparison of D_e values obtained from TD experiments with HTO and NaI tracers.

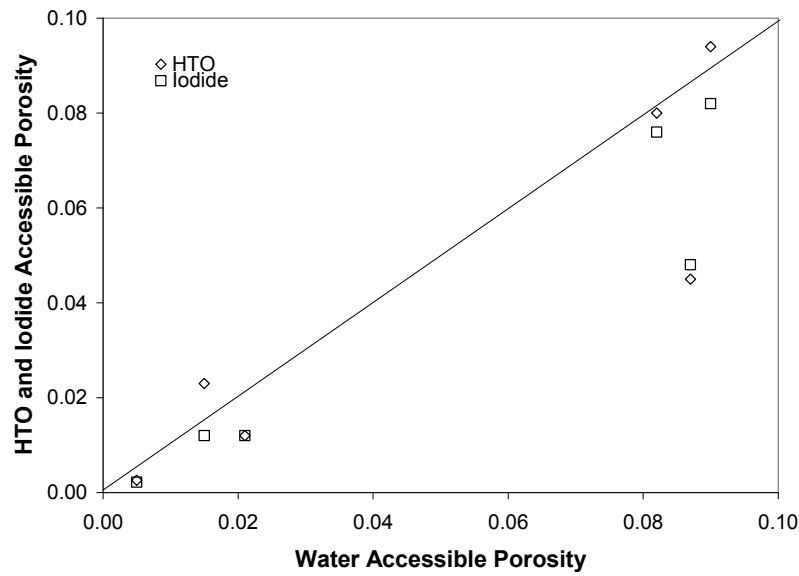


Figure 18 Relationship of ϕ_w to ϕ_i and ϕ_{HTO} from TD measurements.

4.5 Comparison of Radiography and Through Diffusion

Four of the samples that were subjected to TD measurements were also measured using the radiography technique. In comparing the D_e data for the iodide tracer measured by the two different techniques, it is evident that the results are very similar, with radiography and TD measurements differing at most by a factor of 2.25 (see Tables 8 and 9). The D_e data for HTO tracer are also similar to those for the iodide tracer. The greatest differences between D_e for the two tracers are observed from the shale, with D_e for HTO being consistently larger than D_e for iodide by a factor between 1.8 and 3.4. These data are presented versus depth in Figure 19 and it is evident that the D_e data determined by different methods are in good agreement.

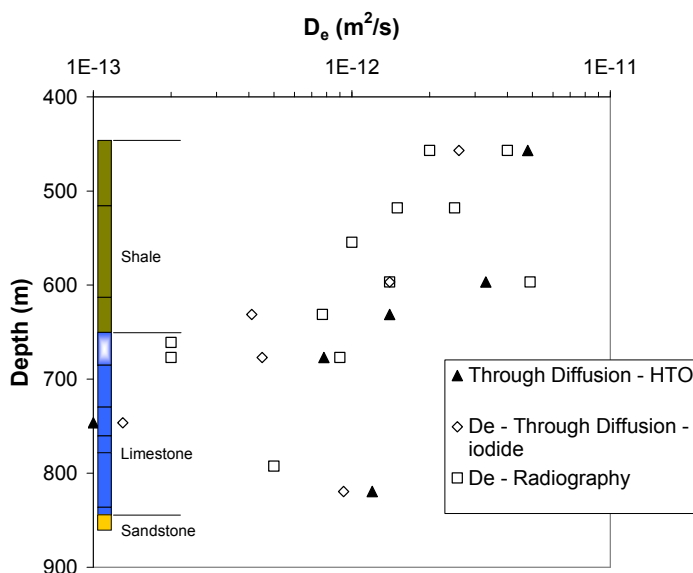


Figure 19 Plots of D_e determined by X-ray radiography and/or TD versus depth (m) from which the rock samples were collected.

4.6 Reproducibility of the TD Measurements

Replicate trials have been conducted on sample OS1-044.57 to evaluate the reproducibility of the method with variable tracer concentration and time. Three replicates were conducted with each tracer. The six trials were completed over a period of one year. The replicate data are presented in Table 10 along with data for iodide and HTO for a second sample (OS1-075.97).

Table 10 Diffusion Properties of Cobourg Formation Limestone from Bowmanville Determined from Replicate TD Measurements using KI and HTO Tracers.

	Diffusion Properties	OS1-44.57	C _{Tracer} ^a (trial) ^b	OS1-75.97	C _{Tracer} ^a (trial) ^b
KI tracer	D _e (m ² /s)	1.2 x 10 ⁻¹²		1.6 x 10 ⁻¹³	
	α	0.031	1.0 M (1)	0.0053	1.0 M (2)
	D _e (m ² /s)	1.2 x 10 ⁻¹²		--	
	α	0.023	0.1 M (3)	--	--
	D _e (m ² /s)	1.3 x 10 ⁻¹²		--	
	α	0.021	1.0 M (6)	--	--
HTO tracer	D _e (m ² /s)	3.6 x 10 ⁻¹²	44,000 Bq/mL	2.6 x 10 ⁻¹³	50,000 Bq/mL (1)
	α	0.038	(4)	0.010	
	D _e (m ² /s)	3.2 x 10 ⁻¹²	4,600 Bq/mL	--	
	α	0.036	(2)	--	--
	D _e (m ² /s)	3.4 x 10 ⁻¹²	4,000 Bq/mL	--	
	α	0.041	(5)	--	--

Notes: ^aConcentration of the tracer during the diffusion experiment; ^bNumbers in parentheses indicate the sequence in which replicate trials were conducted on the same sample. After each trial, tracer was removed by out diffusion before starting a new experiment.

The replicate data reveal that i) D_e and α are independent of the tracer concentration (within experimental errors); ii) the TD method used in this laboratory is reproducible; iii) the limestone samples are stable over a long period of time under these experimental conditions; and iv) based on HTO, the experimental error on replicate analyses is ±5.9% (D_e) and ±6.6% (α).

5 Summary

This report describes a work program designed to provide measurements of diffusion coefficients for selected rock samples from the Ordovician shale and limestone formations intersected by drill hole DGR-2. Diffusion coefficients were measured using two methods: a recently developed X-ray radiography technique and the well established time-lag, or through-diffusion technique. In support of the diffusion coefficient determinations, measurements were conducted to determine the water-loss porosity and pore-water composition.

Water-loss porosity measurements were conducted on two samples from drill hole OS-1, Bowmanville, Ontario, and 12 samples from DGR-2 (Bruce nuclear site, Ontario). The water-loss porosity ranged from 1.3 to 5.3 % for OS-1 limestone samples, from 7.5 to 10% for DGR-2 shale samples, and from 0.4 to 2.3% for DGR-2 limestone samples.

In order to eliminate effects of osmotic gradients between the tracer reservoirs and the natural pore water (brine), the tracer solutions must be prepared in brine, or synthetic pore water (SPW) that has ionic strength similar to the natural pore water. The pore-water composition was determined by the crush-and-leach method for six DGR-2 samples (four shale and two limestone samples). The results indicate that, for the purposes of diffusion measurements, the data can be considered in terms of two separate pore water compositions, one for shale and a second for limestone. The two SPW compositions used for the experiments were based on these data.

The radiography technique provides pore-water diffusion coefficients (D_p) which can be recalculated as effective diffusion coefficients (D_e) for comparison with results from the through-diffusion method. The D_p values obtained by radiography for the DGR-2 samples range from 1.5×10^{-11} to 8.5×10^{-11} m²/s. When these data are recalculated as D_e , they range from 2.0×10^{-13} to 4.9×10^{-12} m²/s. Radiography data are not reported for four of the limestone samples because the signal-to-noise ratio was too low due to their very low porosity. Data were collected from four sets of paired samples (three shale and one limestone), with measurements conducted in directions normal and parallel to the bedding plane. The data indicate that D_p values determined parallel to bedding are larger than those obtained normal to bedding by a factor ranging from 1.7 to 3. Although these results are based on only four sets of paired samples, the results suggest that the diffusion properties of the rocks are anisotropic.

In addition to diffusion coefficient measurements, the radiography technique provides spatially resolved measurements of the tracer-specific (iodide) porosity. A comparison of the water-loss porosity measurements with the iodide-accessible porosity values determined by radiography indicates that iodide-accessible porosity is consistently lower than water-loss porosity for shale samples. This relationship is consistent with solute-specific variations in porosity that are commonly attributed to ion exclusion effects in fine-grained porous media. Spatial variations in iodide-accessible porosity presented either in the form of 2-D images or 1-D profiles provide additional evidence of anisotropy in support of the diffusion coefficient data from paired samples.

In order to provide an independent benchmark for comparison with the radiography data, measurements of D_e were made on six samples by the more conventional through-diffusion method using NaI and tritiated-water (HTO) tracers. Four samples were subjected to measurements with iodide tracer by both techniques. The D_e data for the iodide tracer measured by the two different techniques are very similar, with radiography and TD measurements differing at most by a factor of 2.25. The D_e data for the HTO tracer are also similar to those for the iodide tracer. The greatest differences between D_e for the two tracers are observed from the shale, with D_e for HTO being consistently larger than D_e for iodide by a factor between 1.8 and 3.4. The D_e data determined by different methods are in good agreement.

6 Data Quality and Use

Results of laboratory diffusion testing of DGR-2 core described in this Technical Report are based on testing using new X-ray radiograph techniques and conventional through-diffusion techniques. The results from both techniques are comparable and consequently are considered suitable for assessing the general range of diffusional properties of the Ordovician formations intersecting borehole DGR-2. These data will assist in the development of descriptive hydrogeological models of the Bruce DGR site.

The results of laboratory diffusion testing show a typical range of results reflecting natural lithological and stratigraphic variability of the bedrock formations encountered at the scale of the testing (cm scale). The results generated by laboratory testing described in this Technical Report, are generally consistent with expectations, based on similar testing of these bedrock formations elsewhere in Ontario (Johnson and Wilmot, 1988).

7 References

Al, T., L. Cavé and Y. Xiang, 2007a. Progress Report 1: Measurement of Diffusion Properties by X-Ray Radiography: Surrogate Core Samples from St. Mary's Cement Quarry, Bowmanville, Ontario, Report prepared by University of New Brunswick for Intera Engineering Ltd.

Al, T., Y. Xiang and L.Cavé, 2007b. Progress Report 2: Measurement of Diffusion Properties by X-ray Radiography and by Through-Diffusion Techniques using KI Tracer: Surrogate Core Samples from St. Mary's Cement Quarry, Bowmanville, Ontario, Report prepared by University of New Brunswick for Intera Engineering

Ltd.

Al, T., Y. Xiang, Y. and L. Cavé, 2007c. Progress Report 3: Measurement of Diffusion Properties by X-Ray Radiography and by Through-Diffusion Techniques using Iodide and Tritium Tracers: Core Samples from OS-1 and DGR-2, Report prepared by University of New Brunswick for Intera Engineering Ltd.

Blum, P., 1997. Physical Properties Handbook: A Guide to the Shipboard Measurement of Physical Properties of Deep-Sea Cores. ODP Tech. Note, 26.

Hobbs, M.Y., S.K. Frape, O. Shouakar-Stash and L.R. Kennell, 2008. Phase 1 Regional Hydrogeochemistry Report. OPG's Deep Geologic Repository for Low & Intermediate Level Waste, Supporting Technical Report, Report No. OPG 00216-REP-01300-00006_R00, November.

Intera Engineering Ltd., 2009. Project Quality Plan, DGR Site Characterization, Revision 4, August 14, Ottawa.

Intera Engineering Ltd., 2008. Phase 2 Geoscientific Site Characterization Plan, OPG's Deep Geologic Repository for Low and Intermediate Level Waste, Report INTERA 06-219.50-Phase 2 GSCP-R0, OPG 00216-REP-03902-00006-R00, April, Ottawa.

Intera Engineering Ltd, 2007. Test Plan for Measurement of Diffusion Properties by X-Ray Radiography, TP-06-12, Revision 3, October 9, Ottawa. Report prepared by T. Al and L. Cavé, University of New Brunswick.

Intera Engineering Ltd., 2006. Geoscientific Site Characterization Plan, OPG's Deep Geologic Repository for Low and Intermediate Level Waste, Report INTERA 05-220-1, OPG 00216-REP-03902-00002-R00, April, Ottawa.

Johnson, H.H. and D. J. Wilmot, 1988. Sedimentary Sequence Study: Results of Laboratory Sorption and Diffusion Experiments, Report No. 88-85-K, Ontario Hydro Research Division, Toronto.

Koroleva M. and M. Mazurek, 2006. Characterisation of Pore-Water Compositions in the Queenston Shale (Niagara, Ontario): First Steps Based on a Mineralogical and Leaching Study, RWI Technical Report 2006-03, University of Bern, May 15.

SN-06-12A, Scientific Notebook, Dr. Lisa Cavé, University of New Brunswick.

SN-06-12B, Scientific Notebook, Dr. Yan Xiang, University of New Brunswick.

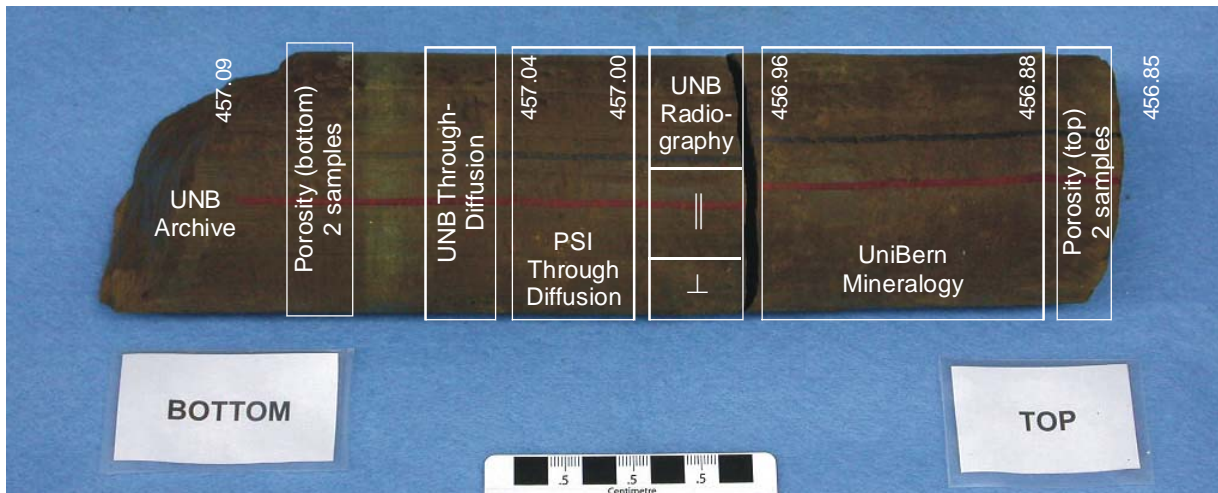
Tidwell, V.C., L.C. Meigs, T. Christian-Frear, and C.M. Boney, 2000. Effects of spatially heterogeneous porosity on matrix diffusion as investigated by X-ray absorption imaging. *Journal of Contaminant Hydrology*, 42, 285–302.

Van Loon, L.R., M. A. Glaus and W. Muller, 2007. Anion exclusion effects in compacted bentonites: Towards a better understanding of anion diffusion, *Applied Geochemistry* Vol. 22, pp. 2536-2552.

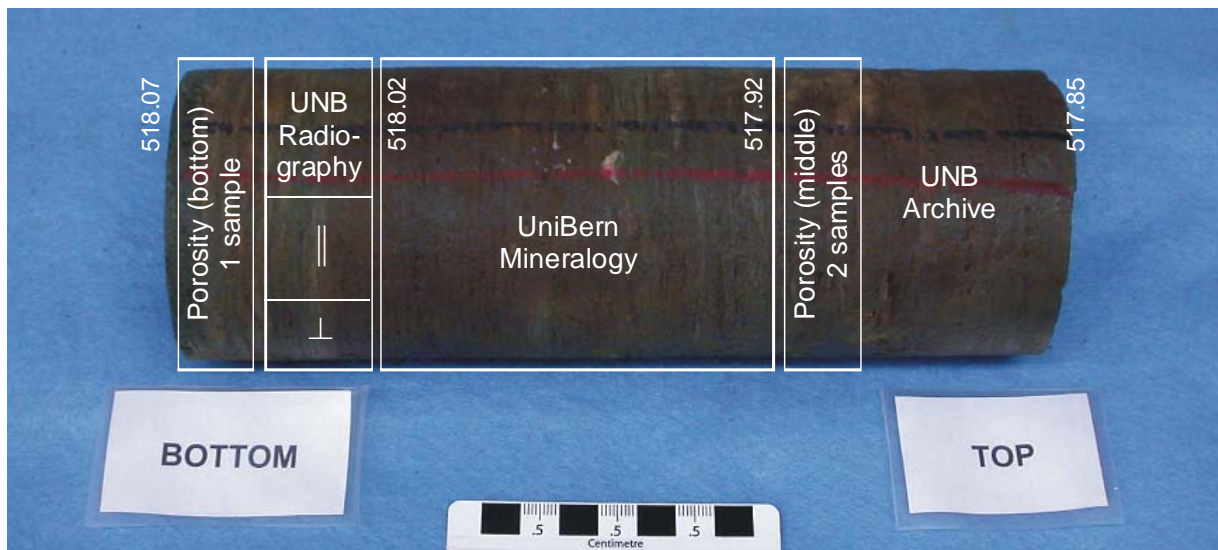
Van Loon, L.R., J.M. Soler and M.H. Bradbury. 2003. Diffusion of HTO, $^{36}\text{Cl}^-$ and $^{125}\text{I}^-$ in Opalinus Clay samples from Mont Terri: Effect of confining pressure. *Journal of Contaminant Hydrology*, Vol. 61, pp. 73–83.

APPENDIX A

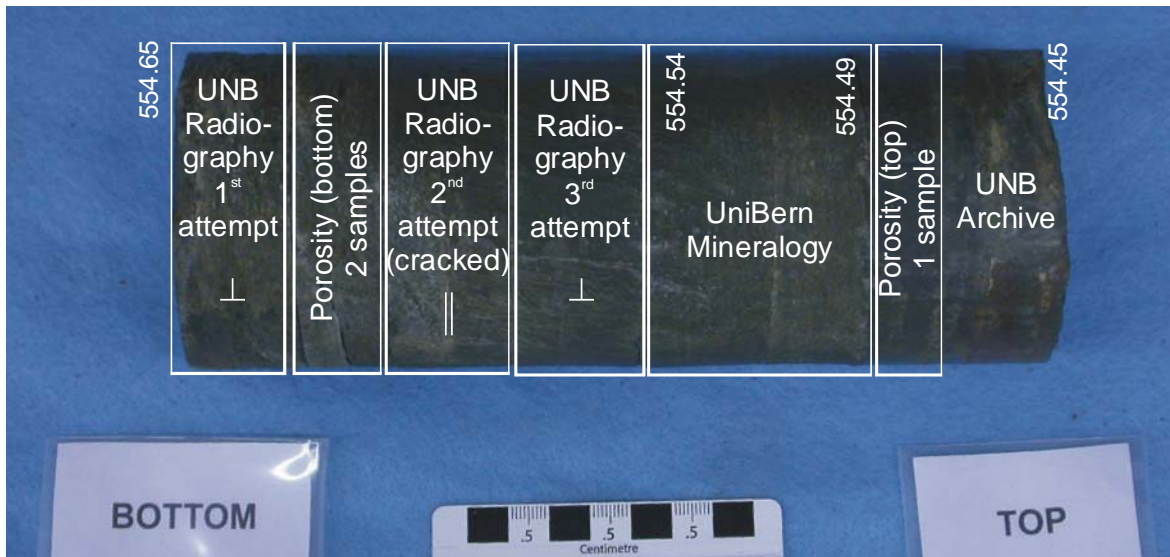
Photographs of the Core Segments



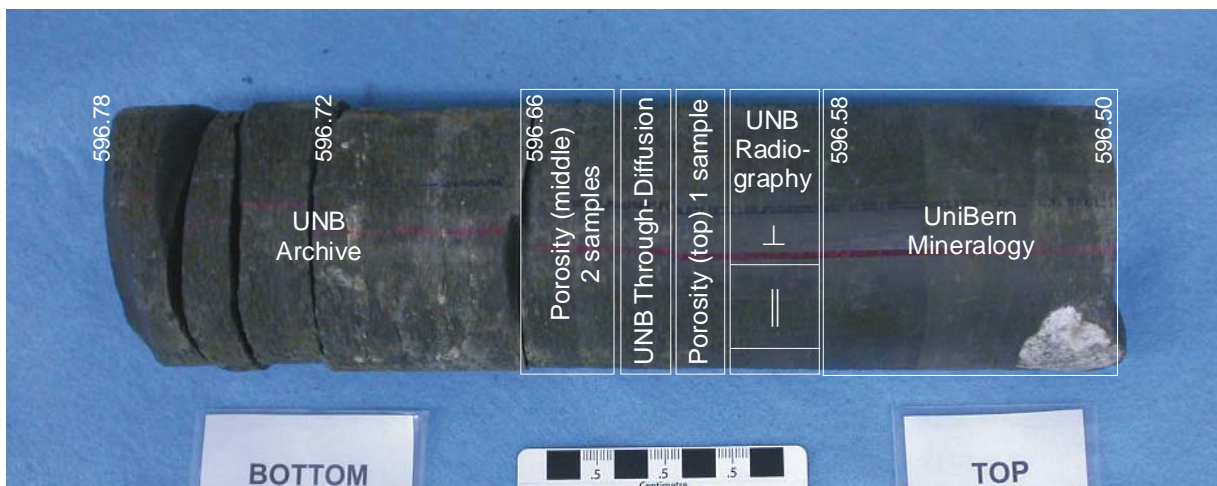
DGR2-456.97
 OPG/INTERA CORE DGR-2 QUEENSTON FORMATION
 DIFFUSION SUBSAMPLES



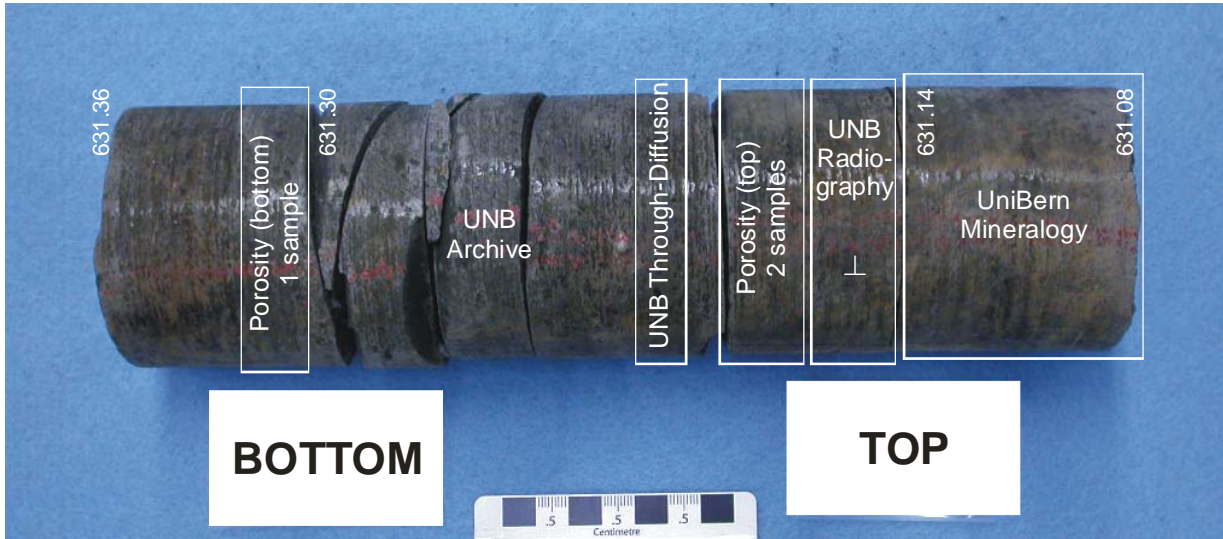
DGR2-517.96
 OPG/INTERA CORE DGR-2 QUEENSTON FORMATION
 DIFFUSION SUBSAMPLES



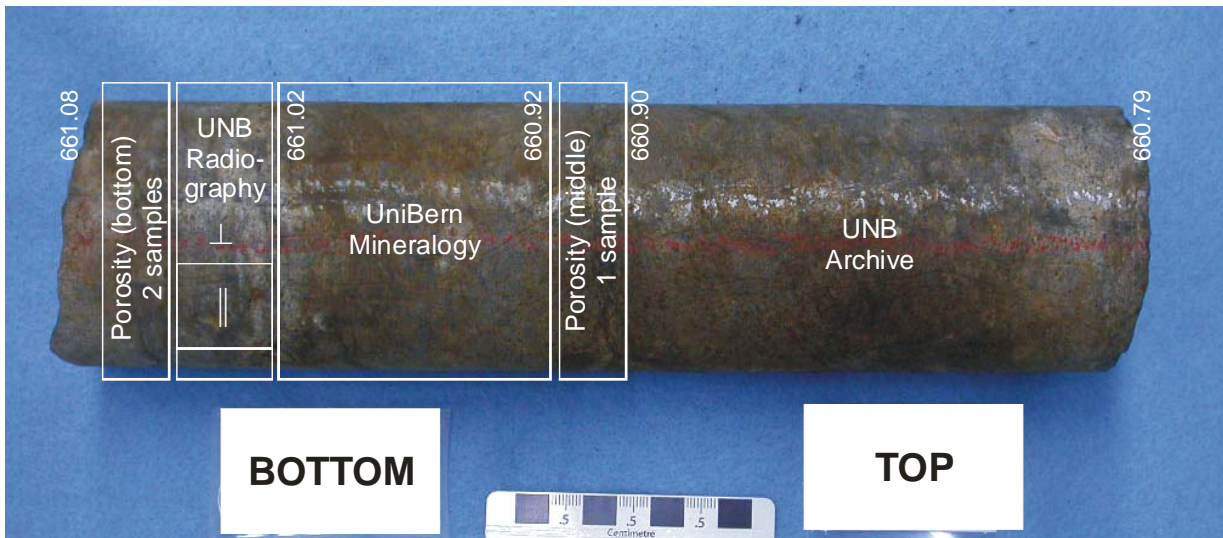
DGR2-554.55
 OPG/INTERA CORE DGR-2 GEORGIAN BAY FORMATION
 DIFFUSION SUBSAMPLES



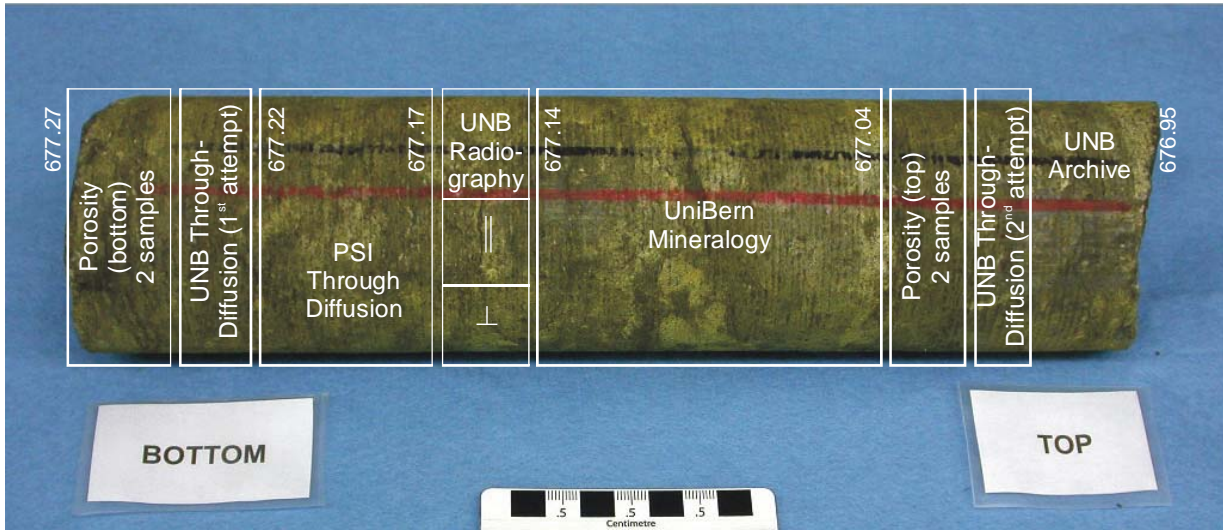
DGR2-596.64
 OPG/INTERA CORE DGR-2 GEORGIAN BAY FORMATION
 DIFFUSION SUBSAMPLES



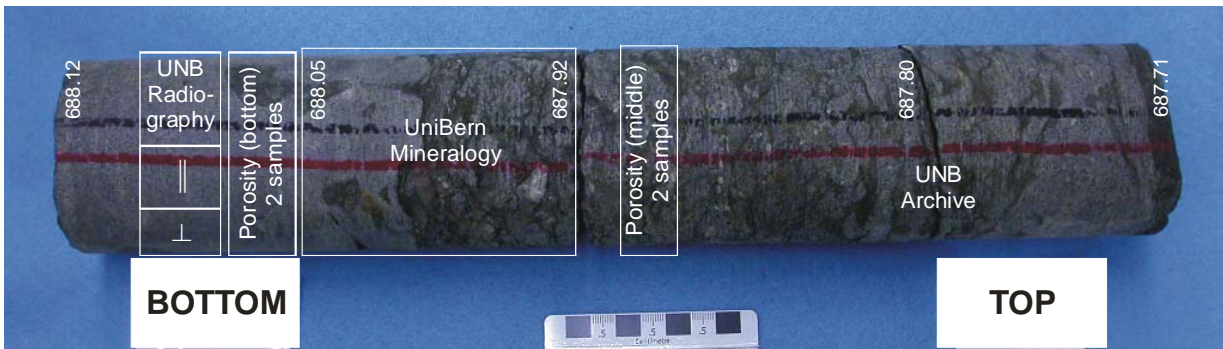
DGR2-631.22
 OPG/INTERA CORE DGR-2 BLUE MOUNTAIN FORMATION
 DIFFUSION SUBSAMPLES



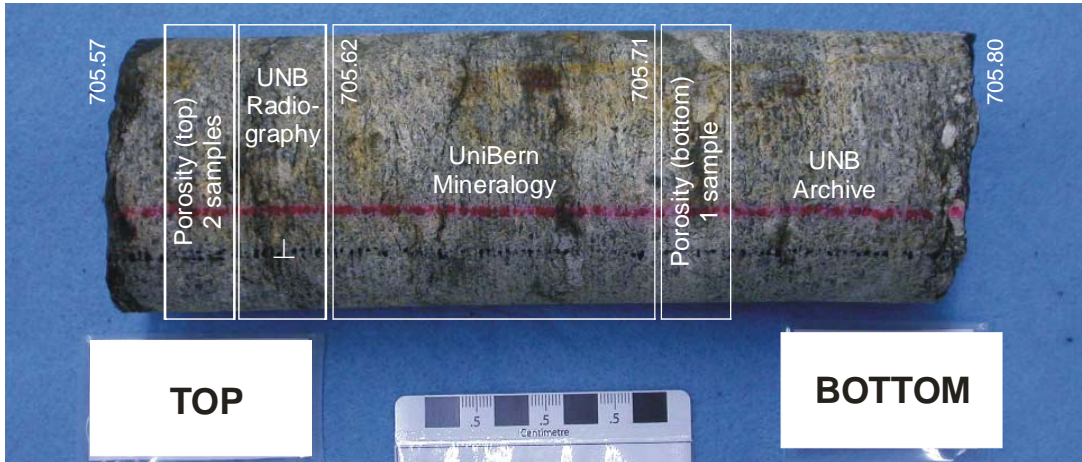
DGR2-660.93
 OPG/INTERA CORE DGR-2 COBOURG FORMATION
 DIFFUSION SUBSAMPLES



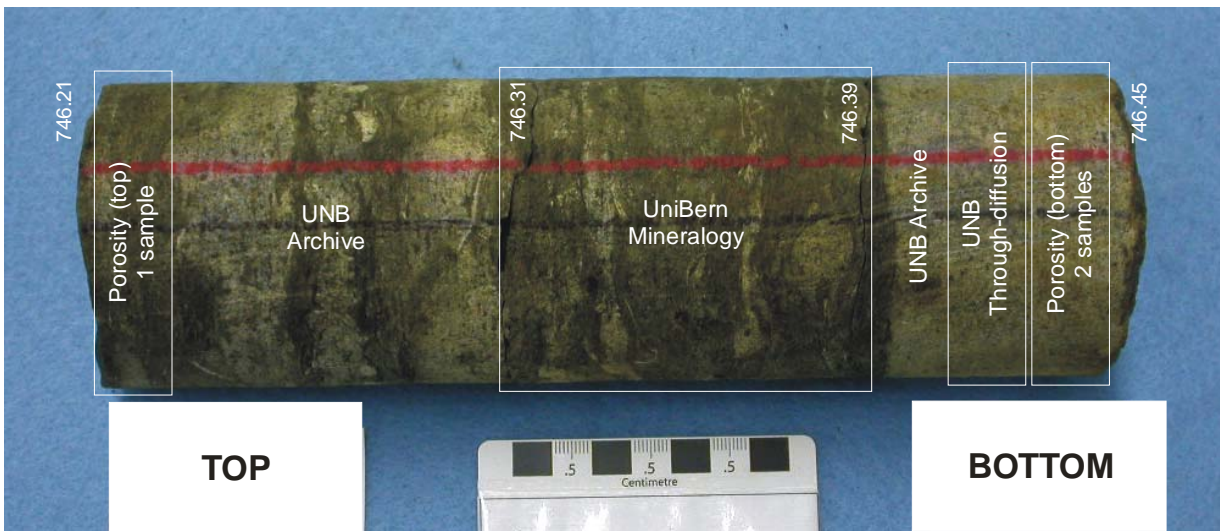
DGR2-677.11
 OPG/INTERA CORE DGR2 COBOURG FORMATION
 DIFFUSION SUBSAMPLES



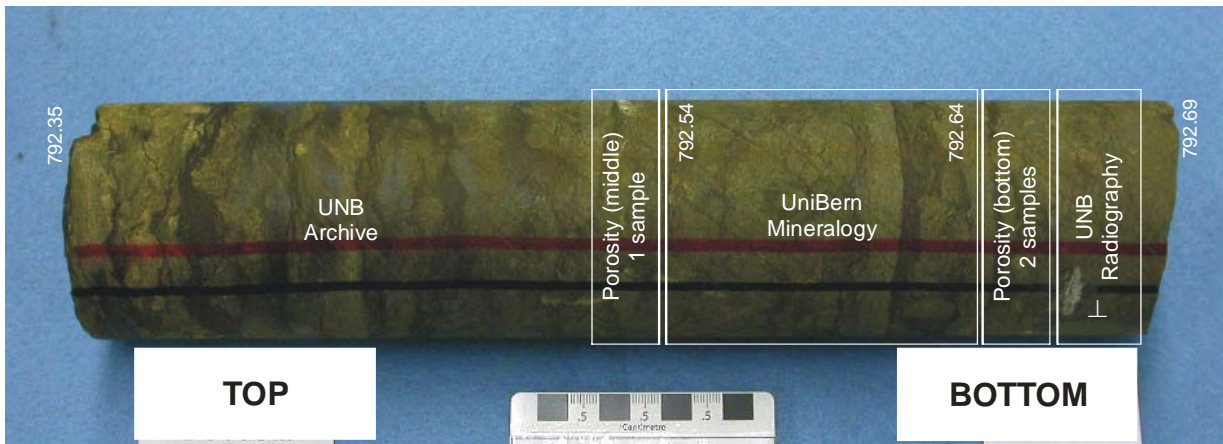
DGR2-687.91
 OPG/INTERA CORE DGR-2 COBOURG FORMATION
 DIFFUSION SUBSAMPLES



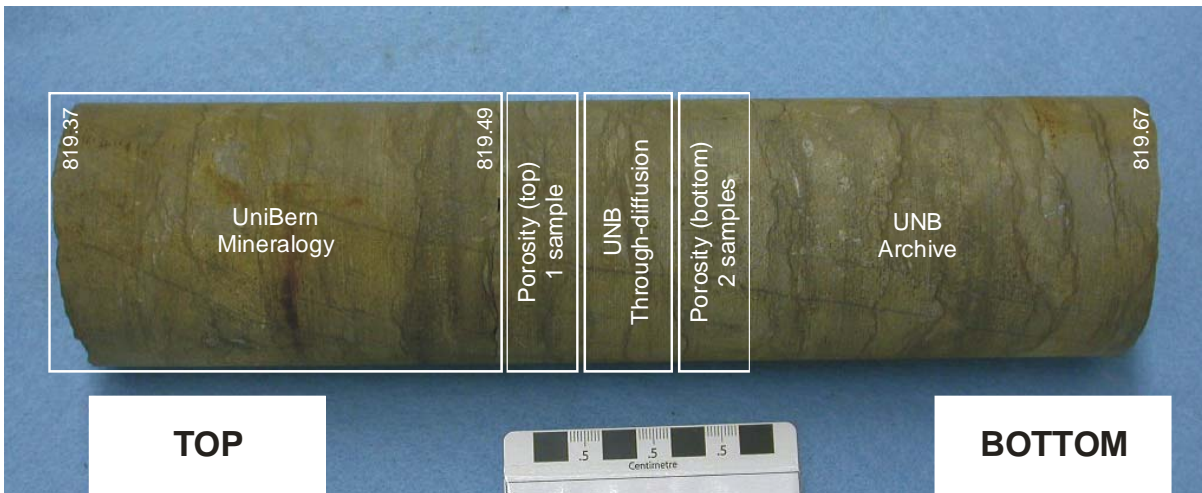
DGR2-705.68
OPG/INTERA CORE DGR-2 SHERMAN FALL FORMATION
DIFFUSION SUBSAMPLES



DGR2-746.33
OPG/INTERA CORE DGR-2 KIRKFIELD FORMATION
DIFFUSION SUBSAMPLES



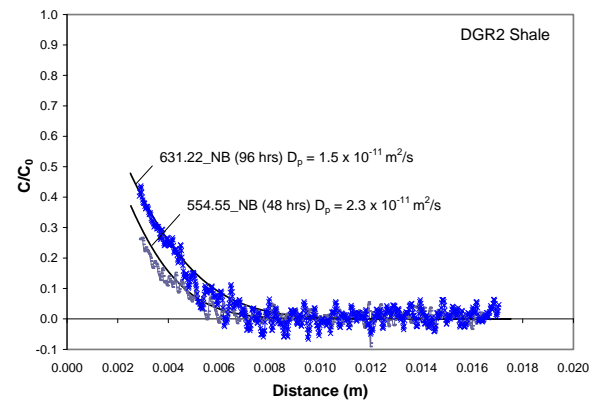
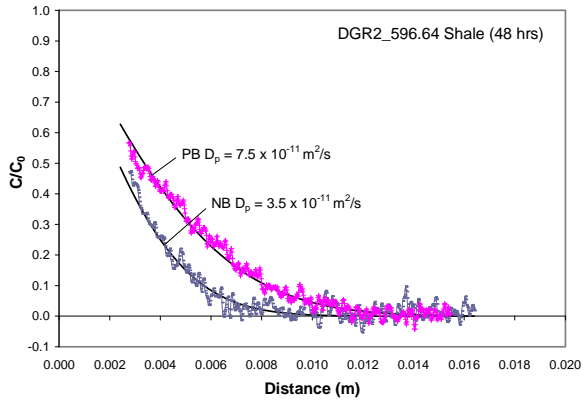
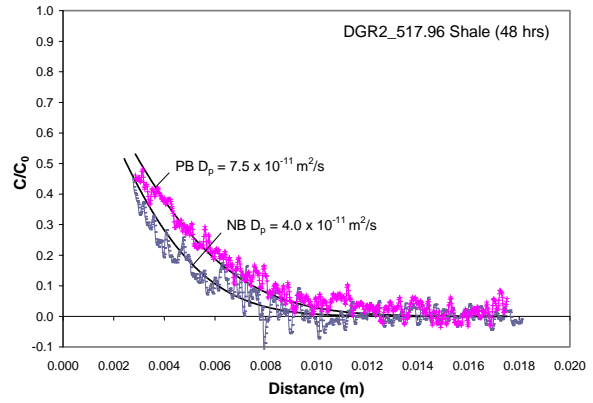
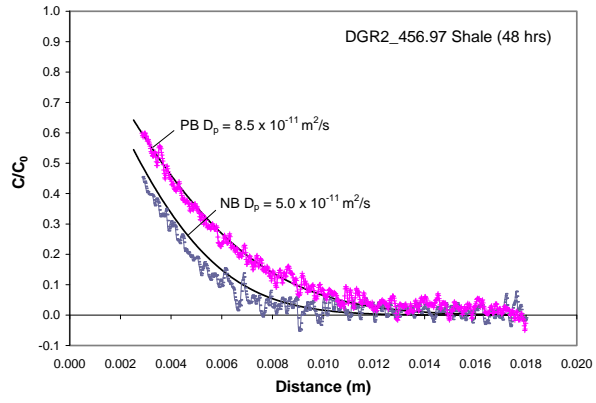
DGR2-792.52
OPG/INTERA CORE DGR-2 GULL RIVER FORMATION
DIFFUSION SUBSAMPLES



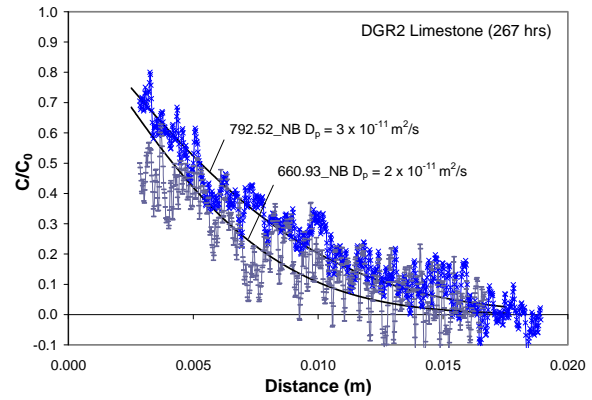
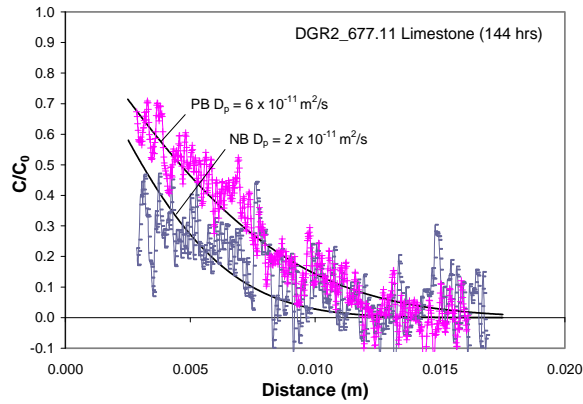
DGR2-819.52
OPG/INTERA CORE DGR-2 GULL RIVER FORMATION
DIFFUSION SUBSAMPLES

APPENDIX B

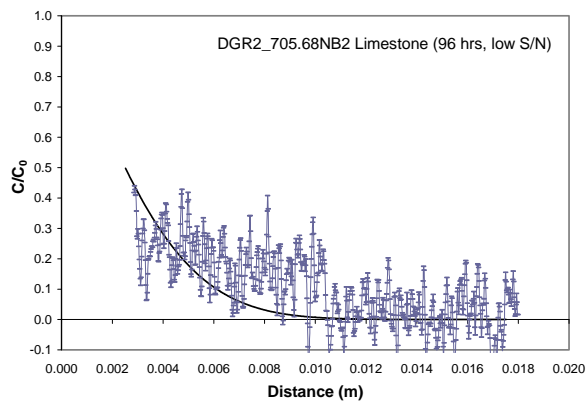
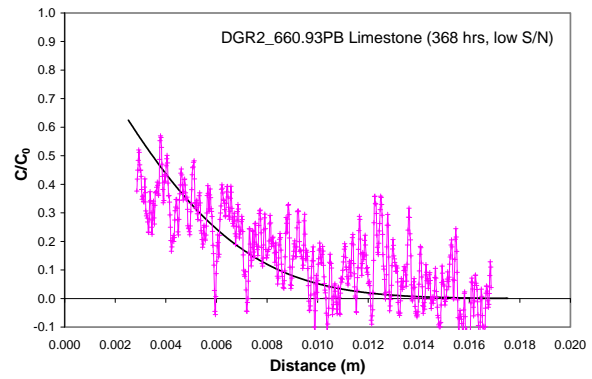
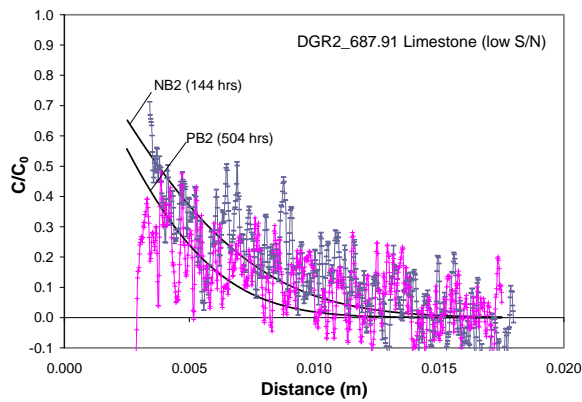
One-Dimensional Diffusion Profiles Determined by X-Ray Radiography for DGR-2 Samples



1D C/C_0 iodide-tracer diffusion profiles for DGR-2 shale samples



1D C/C_0 iodide-tracer diffusion profiles for DGR-2 limestone samples (reported data)



1D C/C_0 iodide-tracer diffusion profiles for DGR-2 limestone samples (unreported data)